NHC-Ni Nanoclusters covalently ligated on Carbon Nanotubes: Highly Active Electrocatalysts for the Oxygen Evolution Reaction

Amalia Rapakousiou*[,†], Savvas G. Chalkidis[‡], Michail P. Minadakis[†], María Luisa Ruiz-González[§], Cristina Navio[‖], Georgios C. Vougioukalakis*[,‡], Nikos Tagmatarchis*[,†]

†Theoretical and Physical Chemistry Institute, National Hellenic Research Foundation, 48 Vassileos Constantinou Avenue, Athens 11635, Greece

‡Laboratory of Organic Chemistry, Department of Chemistry, National and Kapodistrian University of Athens, 15771, Athens, Greece

§Departamento de Química Inorgánica, Universidad Complutense de Madrid, Madrid, Spain

‖IMDEA Nanoscience, C/Faraday 9, Ciudad Universitaria de Cantoblanco, 28049 Madrid, Spain

SUPPLEMENTARY INFORMATION

Corresponding author: arapak@eie.gr

Materials and Methods. All solvents and reagents were obtained from commercial suppliers and used as received unless otherwise stated. Aligned multi-walled carbon nanotubes / MWCNTs were purchased from NanoAmor (Los Alamos, NM, USA). The course of the organic reactions was monitored via thin-layer chromatography (TLC), using aluminum sheets (0.2 mm) coated with silica gel 60 with a fluorescence indicator (silica gel 60 F_{254}). The developed TLC plates were analysed by UV lamp (254 nm and 365 nm) or by potassium permanganate solution for visualization. Purification of the products was carried out by flash column chromatography, using silica gel 60 (230−400 mesh). **Nuclear Magnetic Resonance spectra (^{1}H-NMR, ^{13}C-NMR, ^{19}F-NMR, and ^{1}H, ^{13}C-HSQC)** were obtained with a Bruker Avance 500 MHz, a Bruker Avance 400 MHz or a Varian Mercury 200 MHz spectrometer, using $CDCl_3$ as solvent and its residual solvent peak as a reference. Data are reported as follows: chemical shift, multiplicity (s = singlet, d = doublet, t = triplet, dd = doublet of doublets, ddt = doublet of doublet of triplets, tt = triplet of triplets, br = broad, m = multiplet), coupling constant (Hz), and integration. **High-resolution mass spectra (HRMS)** were recorded in a QTOF maxis impact (Bruker, Billerica, MA, USA) spectrometer with electron spray ionization (ESI). **Probe sonication** was performed with a Sonopuls Bandelin Ultrasonic Homogenizer HD 3200 equipped with a flat head probe (VS-70T), running at 35% (87.5 W) of the maximum power (250 W). **Mid-infrared spectra** in the region 675-4500 cm^{-1} were acquired on a Fourier transform IR spectrometer (Tensor II, Bruker Optics, Billerica, MA, USA) equipped with a single reflection Ge ATR crystal (Miracle by PIKE Technologies, Madison, WI, USA). Typically, 100 scans were acquired at 4 cm^{-1} resolution. **Micro-Raman scattering** measurements were performed at compressed powder samples, at room temperature, in the backscattering geometry using a RENISHAW inVia Reflex Raman spectrometer (Wotton-under-edge, UK) equipped with a CCD camera and a Leica microscope. A 2400 lines mm^{-1} grating was used for all measurements, providing a spectral resolution of ± 1 cm^{-1}. As the excitation source, an Ar^{+} laser line of 514 nm was used. Measurements were taken with varying numbers of accumulations, each with a 10 second exposure and laser power ~0.3 mW cm^{-2} to avoid overheating of the samples. The laser spot was focused on the sample surface using a long working distance Leica 50x objective lens. Raman spectra were collected after map image acquisition was conducted on five (5) areas of the sample (605 measurements) and recorded with Peltier cooled CCD camera. The intensity ratio D/G was obtained by taking the integrated peak intensities, following baseline correction. For the mapping recordings: 5 areas (30 μm x

30 μm each) were measured with a 3 μm step. for every sample (605 measurements), and we include the most representative map, closest to the total average with respect either to the intensity ratio D/G, or the G and D bands position. The data were collected and analyzed with Renishaw Wire 3.4 and Origin 8 Pro software. **Thermogravimetric analysis** was performed using a TGA Q500 V20.2 Build 27 instrument by TA (Boston, MA, USA) in an inert atmosphere of nitrogen (purity >99.999%). In a typical experiment, 2 mg of the material were placed in the platinum pan and the temperature was equilibrated at 40 ^{o}C. Subsequently, the temperature was increased to 800 ^{o}C at a rate of 10 ^{o}C/min and the weight changes were recorded as a function of temperature. Derivatives of weight loss to temperature were used to assess the thermal decomposition profile of each material. **XPS measurements** were performed under Ultra High Vacuum conditions (UHV, with a base pressure of 4×10^{-10} mbar), using a monochromatic Al Kα line as exciting photon source for core level analysis (hν = 1486.7 eV). The emitted photoelectrons were collected in a hemispherical energy analyzer (SPHERA-U7, pass energy set to 20 eV for the XPS measurements to have a resolution of 0.6 eV) and to compensate the built-up charge on the sample surface it was necessary (for the XPS measurements) the use of a Flood Gun (FG-500, Specs), with low energy electrons of 3 eV and 40 μA. The sp^2 component of the C 1s core level centered in 284.4 eV was used as a binding energy reference. **Samples for electron microscopy** were deposited on carbon-coated nickel grids by drop-casting butanol suspensions of functionalized MWCNTs. The **Transmission Electron Microscopy (TEM)** imaging study at low magnification was performed with a JEOL 2100 transmission electron microscope operated at 200 kV. **High Resolution Transmission Electron Microscopy (HRTEM)** images were obtained in a JEOL-JEM GRAND ARM 300cF microscope equipped with a Cs Corrector (ETA-JEOL). A precise measurement of the aberrations and an optimized correction has been done using the corrector control software JEOL COSMO. The accelerating voltage was set to 60 kV in order to minimize the sample damage. The HRTEM images were acquired by a Gatan OneView camera (4096 x 4096 pixels). **EDS** spectra were acquired in STEM mode using a SDD CENTURIO detector.

Oxygen evolution reaction (OER) measurements were carried out on an Autolab PGSTAT128N (Metrohm, Herisau, Switzerland) potentiostat/galvanostat in a standard three-compartment electrochemical cell. Platinum foil was used as the counter-electrode, a ring rotating disk electrode (RRDE) with glassy carbon (GC) disk (geometric surface area: 0.196 cm^2) was the working

electrode and Hg/HgO (aqueous 0.1 M KOH as filling solution) was used as the reference electrode. LSV polarization curves were recorded at ambient temperature in freshly prepared, N_2-saturated aqueous 0.1 M KOH and/or 1 M KOH, with a scan rate of 5 mV s^{-1}. The catalyst ink was prepared by dispersing 1.0 mg of the catalytic powder in a 250 μL mixture of deionized water, isopropanol and 5% Nafion (v/v/v = 4:1:0.02) and bath sonicate for 30 min prior to use. Before casting the electrocatalytic ink on the electrode surface, the working electrode was polished with 1 mm diamond paste and fine Al_2O_3 powder and was thoroughly rinsed with deionized water. Afterwards, 8.5 μL aliquots of the electrocatalyst ink was casted on the electrode surface and were firstly left to dry at room temperature then under N_2 stream.

All measured potential values were reported versus the reversible hydrogen electrode (RHE) using the following equation:

$E_{RHE} = E_{Hg/HgO} + 0.165 + 0.059pH$.

Electrochemical impedance spectroscopy (EIS) was conducted from 10^5 to 10^{-1} Hz with an AC amplitude of 0.01 V. EIS measurements were recorded on potential values where significant OER current was produced, corresponding to 2 mA cm^{-2} for the study on GC.

For the calculation of double layer capacitance (C_{dl}), cyclic voltammograms were recorded at a 300-400 mV window in a region where no Faradaic processes take place and with scan rates ranging from 50-500 mV s^{-1}. It is known that charging current (i_c) is directly proportional to the scan rate (v), with the slope (b) corresponding to C_{dl} ($i_c = b \cdot v$)[S1-2]. Therefore, the ½ Δi ($\Delta i = i_{anode} - i_{cathode}$) was plotted against the scan rate and an average value of C_{dl} was calculated. For the calculation of electrochemically active surface area (ECSA), the roughness factor (RF) should initially be estimated. By taking into consideration a 40 μF cm^{-2} value for the specific capacitance of a flat electrode (C_s), roughness factor was calculated by the equation: $RF = C_{dl}/C_s$. Finally, ECSA was calculated via the equation: $ECSA = RF \cdot A_{Geom}$.

1. Experimental Procedures & Characterization

Synthesis and characterization of 5

2,3-bis(mesitylamino)propan-1-ol (1)

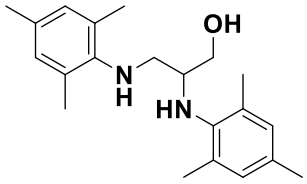

A round bottom flask was charged with 2,3-dibromopropan-1-ol (5.01 g, 23.0 mmol, 1.0 eq.) and 2,4,6-trimethylaniline (12.44 g, 92 mmol, 4 eq.) and heated to 120 °C for 20 h under vigorous stirring. After cooling to room temperature, aqueous NaOH solution (1.7 M, 200 mL) was added. The mixture was extracted with CH_2Cl_2 (3 x 200 mL), and the combined organic layers were dried over $MgSO_4$ and concentrated under reduced pressure to afford the crude product as a dark brown liquid. Purification was carried out via column chromatography (PE/EtOAc: 3/1) to afford the product as a brown solid (4.15 g, 13.8 mmol, 60%). ^{1}H NMR (400 MHz, $CDCl_3$) δ 6.84 (s, 2H), 6.82 (s, 2H), 4.01 – 3.94 (m, 1H), 3.85 (dd, *J* = 11.3, 4.0 Hz, 1H), 3.62 (br, 3H), 3.43 – 3.37 (m, 1H), 3.23 (dd, *J* = 12.0, 4.9 Hz, 1H), 3.04 – 2.96 (m, 1H), 2.30 (s, 6H), 2.24 (s, 3H), 2.23 (s, 3H), 2.18 (s, 6H). ^{13}C NMR (100 MHz, $CDCl_3$) δ = 142.7, 142.0, 132.7, 131.1, 130.8, 129.9, 129.7, 128.9, 66.3, 57.1, 52.5, 20.7, 20.6, 19.1, 17.9. The spectral data are in accordance with the literature[S3].

N^1, N^2-dimesityl-3-(prop-2-yn-1-yloxy)propane-1,2-diamine (2)

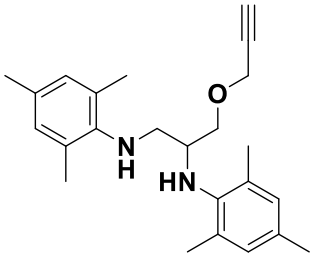

A round bottom flask was charged with **1** (2.40 g, 7.35 mmol, 1 eq.), propargyl bromide (80% in toluene, 2.19 g, 14.7 mmol, 2 eq.) and dry THF (34 mL). Sodium hydride (60% in mineral oil, 0.88 g, 22.1 mmol, 3 eq.) was added slowly and the mixture stirred at 40 °C for 16 h. After cooling to room temperature, water (10 mL) was added, and the mixture was concentrated to remove THF. The remaining aqueous mixture was extracted with CH_2Cl_2 (3 x 30 mL). The combined organic layers were dried over $MgSO_4$ and concentrated under reduced pressure. Purification was carried out via column chromatography (PE/EtOAc: 15/1) to afford the product as a yellow solid (2.20 g, 6.1 mmol, 83%). ^{1}H NMR (400 MHz, $CDCl_3$) δ 6.84 (s, 4H), 4.30 – 4.07 (m, 2H), 3.93 – 3.42 (m, 5H), 3.39 – 3.19 (m, 1H), 3.14 – 3.00 (m, 1H), 2.53 – 2.39 (m, 1H), 2.37 – 2.06 (m, 18H). ^{13}C NMR (100 MHz, $CDCl_3$) δ = 143.7, 141.7, 131.4, 131.0, 130.0, 129.7, 129.5, 129.4, 79.6, 74.9, 70.4, 58.6, 56.6, 50.7, 20.7, 18.9, 18.5. The spectral data are in accordance with the literature[S4].

1,3-dimesityl-4-[(prop-2-yn-1-yloxy)methyl]-4,5-dihydro-1H-imidazol-3-ium tetrafluoroborate (3)

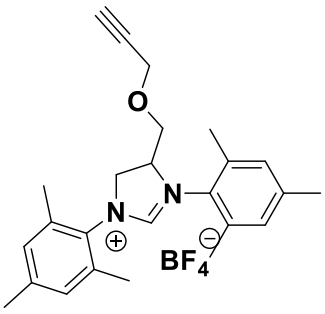

A Schlenk tube was charged with **2** (1.5 g, 4.1 mmol,1 equiv.), triethyl orthoformate (2 mL, 12.3 mmol, 3 equiv.) and NH_4BF_4 (0.475 g, 4.53 mmol, 1.1 equiv.). The reaction was stirred at 120 °C for 24 h. Then the reaction mixture was cooled to room temperature, and the reaction mixture was concentrated under reduced pressure. The resultant brown solid was washed several times with *n*-pentane and Et_2O. CH_2Cl_2 was added (5 ml) and the mixture was passed through a cotton plug to remove remaining NH_4BF_4. The solvent was concentrated under reduced pressure to afford the product as a brown solid (1.73 g, 3.74 mmol, 91% yield). ^{1}H NMR (400 MHz. CDCl3): δ 7.82 (s, 1H), 6.97 (s, 4H), 5.23 (dd, *J* = 12.9, 7.0 Hz, 1H), 4.78 – 4.68 (m, 1H), 4.38 (dd, *J* = 12.2, 7.6 Hz, 1H), 3.71 (d, *J* = 11.2 Hz, 1H), 3.59 (d, *J* = 11.4 Hz, 1H), 2.46 – 2.42 (m, 1H), 2.41 – 2.26 (m, 18H). ^{13}C NMR (50 MHz, $CDCl_3$) δ 157.9, 141.0, 140.7, 135.8, 135.7, 135.4, 130.8, 130.3, 130.2, 128.3, 78.1, 76.0, 66.3, 64.0, 58.6, 53.0, 21.2, 21.1, 18.4, 17.8, 17.8. ^{19}F NMR (188 MHz, $CDCl_3$) = δ -153.18. The spectral data are in accordance with the literature[S5].

NHC-precursor 5

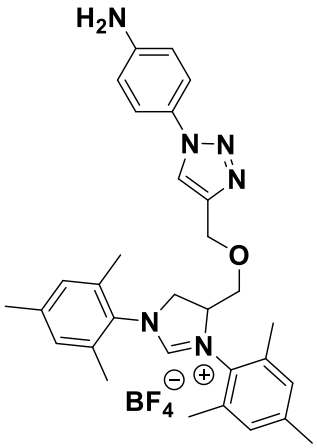

A vial was charged with **3** (0.1 g, 0.216 mmol), p-azidoaniline (0.029 g, 0,216 mmol) and CuBr (0.019 g, 0.13 mmol). THF (10 mL) was added and the reaction was stirred at 50 °C for 24 h, until p-azidoaniline is not present on the developed TLC plate (CH_2Cl_2). Then, the reaction mixture was concentrated and passed through celite with CH_2Cl_2 to remove insoluble material. The solution was transferred into a separatory funnel and washed with 10% ammonia solution. The aqueous phase was extracted with CH_2Cl_2 (3 x 10 mL). The combined organic phases were washed water (3 x 10 mL) and dried over $MgSO_4$. The solvent was concentrated under reduced pressure affording the product as a brown solid (0.096 g, 0.162 mmol, 75%). ^{1}H NMR (400 MHz, DMSO-d_6) δ 9.02 (s, 1H), 8.44 (s, 1H), 7.44 (d, *J* = 8.8 Hz, 2H), 7.17 – 6.88 (m, 4H), 6.70 (d, *J* = 8.7 Hz, 2H), 5.49 (br, 2H), 5.06 (ddt, *J* = 9.8, 7.3, 3.8 Hz, 1H), 4.65 (s, 2H), 4.57 (t, *J* = 12.0 Hz, 1H), 4.28 (dd, *J* = 11.7, 7.1 Hz, 1H), 3.62 (dd, *J* = 11.4, 3.0 Hz, 1H), 3.50 (dd, *J* = 11.3, 1.9 Hz, 1H), 2.35 (s, 3H), 2.33 – 2.30 (m, 6H), 2.26 (s, 3H), 2.25 (s, 3H), 2.15 (s, 3H). ^{13}C NMR (126 MHz, DMSO) δ 159.9, 148.8, 143.2, 139.4, 139.0, 136.0, 135.3, 135.1, 135.0, 130.5, 129.5, 129.3, 129.2, 129.1, 128.8, 125.7, 121.9, 121.1, 113.8, 66.4, 63.2, 62.4, 51.7, 20.2, 20.1, 17.6, 16.9, 16.8, 16.7. ^{19}F NMR (188 MHz, $CDCl_3$) = δ -153.05. HRMS (ESI-TOF): m/z $[M - BF_4]^+$ Calcd. for $C_{31}H_{37}N_6O^+$ 509.3023, Found 509.3029.

Synthesis of NHC-Cu(I) (6)

(4-(((1-(4-aminophenyl)-1H-1,2,3-triazol-4-yl)methoxy)methyl)-1,3-dimesitylimidazolidin-2-yl)copper(I) chloride (6)

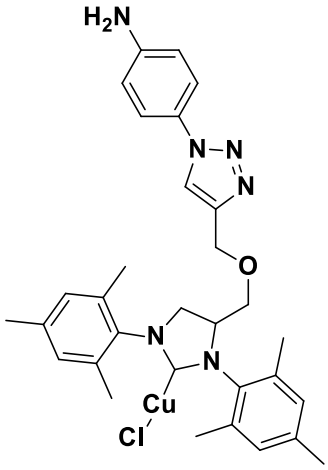

A vial was charged with **5** (0.05 g, 0.083 mmol), CuCl (0.083 g, 0.083 mmol) and K_2CO_3 (0.023 g, 0.167 mmol). The mixture was dissolved in acetone (1.0 mL) and stirred at 60 °C for 24 hours. The solution was then passed through a celite plug with CH_2Cl_2 (3 x 5 mL). The solvent was concentrated under reduced pressure and a brown solid was collected, which was washed with *n*-pentane (0.046 g, 0.075 mmol, 90%). ^{1}H NMR (400 MHz, CDCl3) δ 7.69 (s, 1H), 7.43 (d, *J* = 8.4 Hz, 2H), 6.97 – 6.86 (m, 4H), 6.77 (d, *J* = 8.3 Hz, 2H), 4.67 (s, 2H), 4.45 (ddt, *J* = 11.7, 7.8, 3.9 Hz, 1H), 4.04 – 3.87 (m, 4H), 3.60 (tt, J = 10.0, 5.2 Hz, 2H), 2.43 (s, 3H), 2.27 (s, 12H), 2.20 (s, 3H). ^{13}C NMR (101 MHz, $CDCl_3$) δ 203.4, 147.4, 144.3, 138.6, 138.4, 136.8, 135.9, 135.3, 135.2, 135.1, 133.8, 130.1, 130.0, 129.8, 129.7, 128.4, 122.3, 121.1, 115.4, 69.0, 64.6, 62.8, 53.1, 21.1, 21.1, 18.7, 18.3, 18.1, 18.00. HRMS (ESI-TOF): m/z $[M – Cl(MeCN)]^+$ Calcd. for $C_{33}H_{39}CuN_7O^+$ 612,2507, Found: 612,2505.

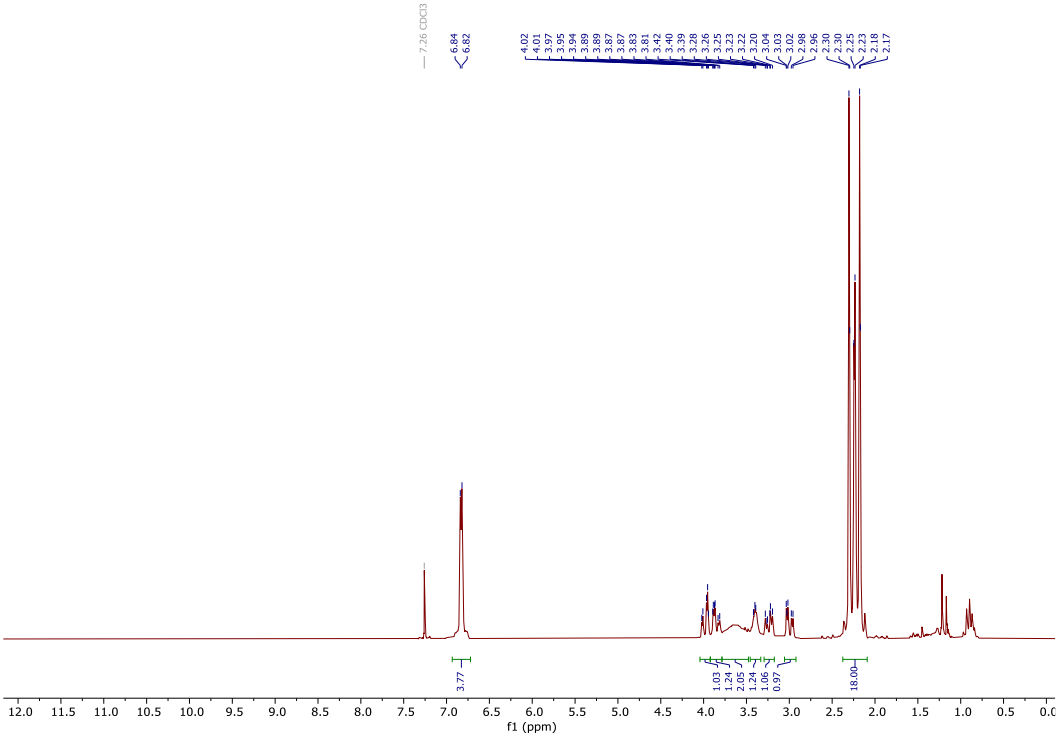

Fig. S1. ^{1}H-NMR spectrum of compound **1.**

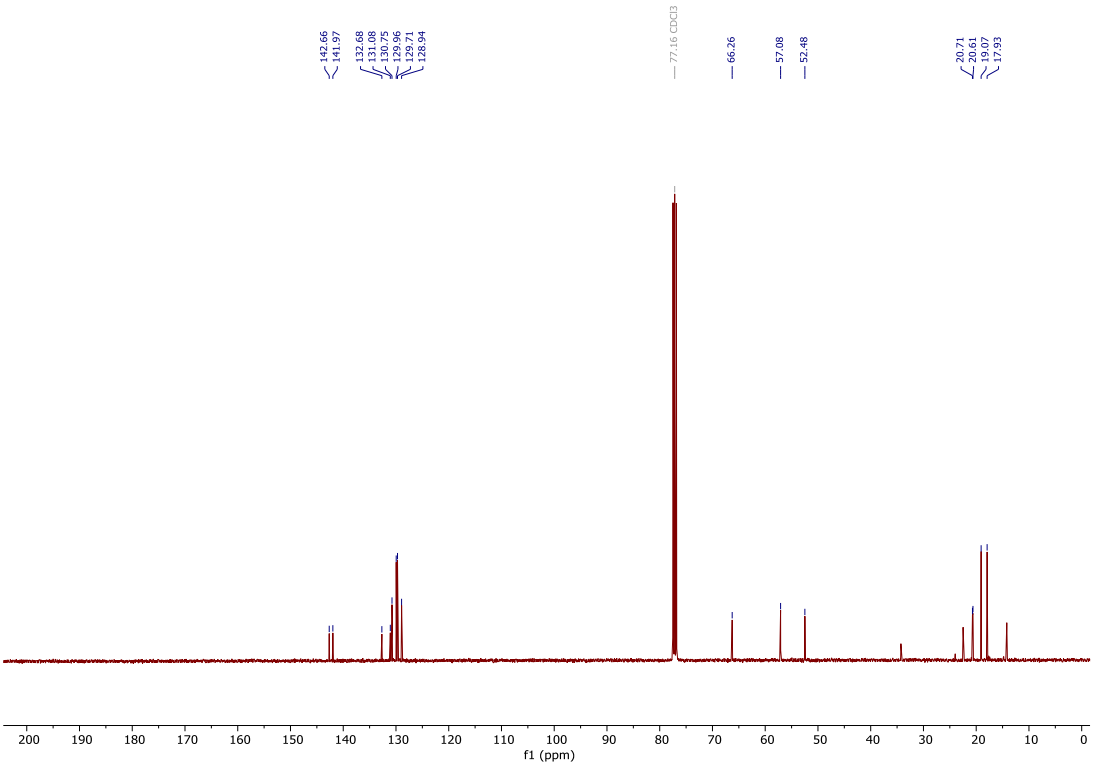

Fig. S2. ^{13}C-NMR spectrum of compound **1.**

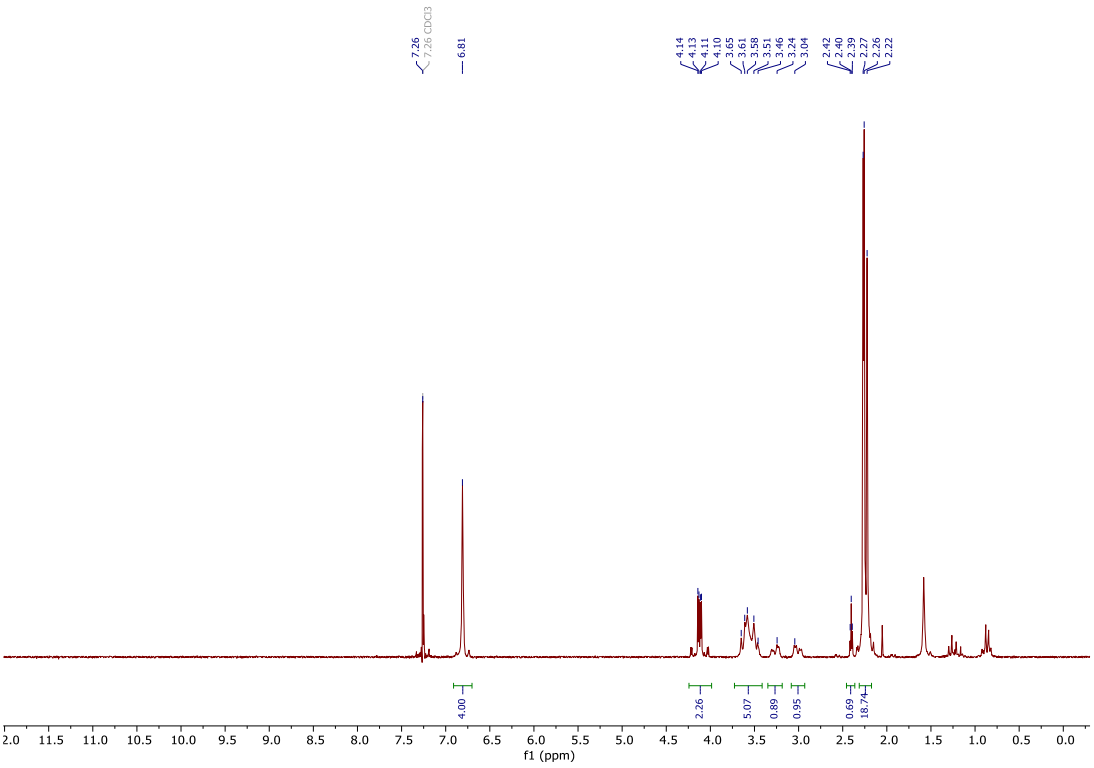

Fig. S3. ^{1}H-NMR spectrum of compound **2.**

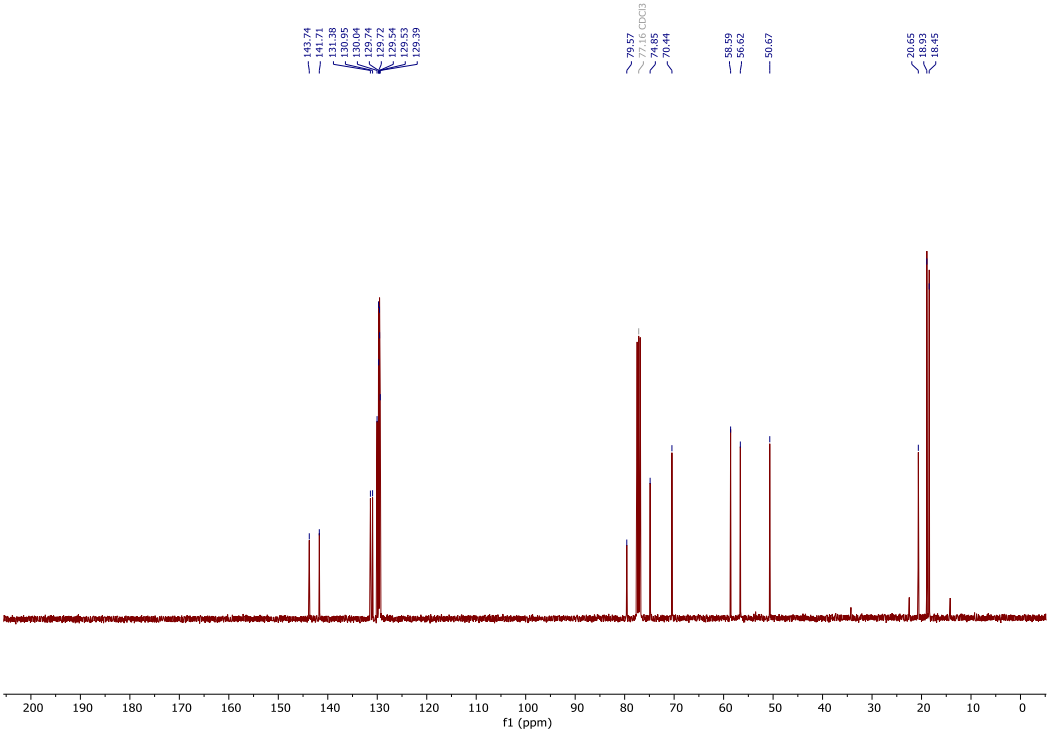

Fig. S4. ^{13}C-NMR spectrum of compound **2.**

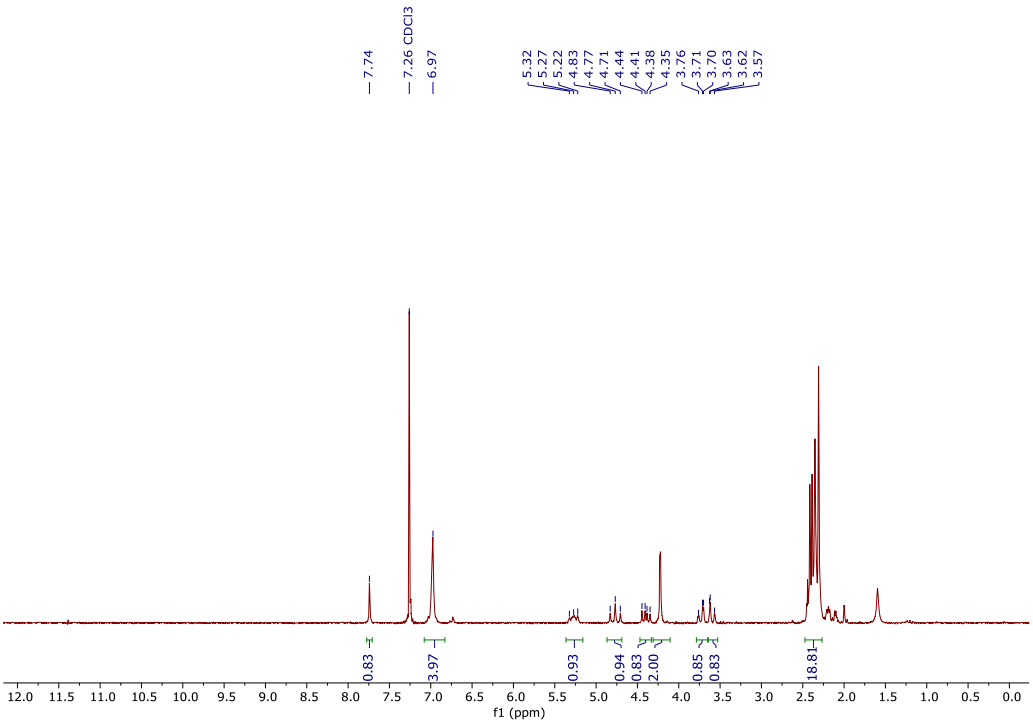

Fig. S5. ^{1}H-NMR spectrum of compound **3.**

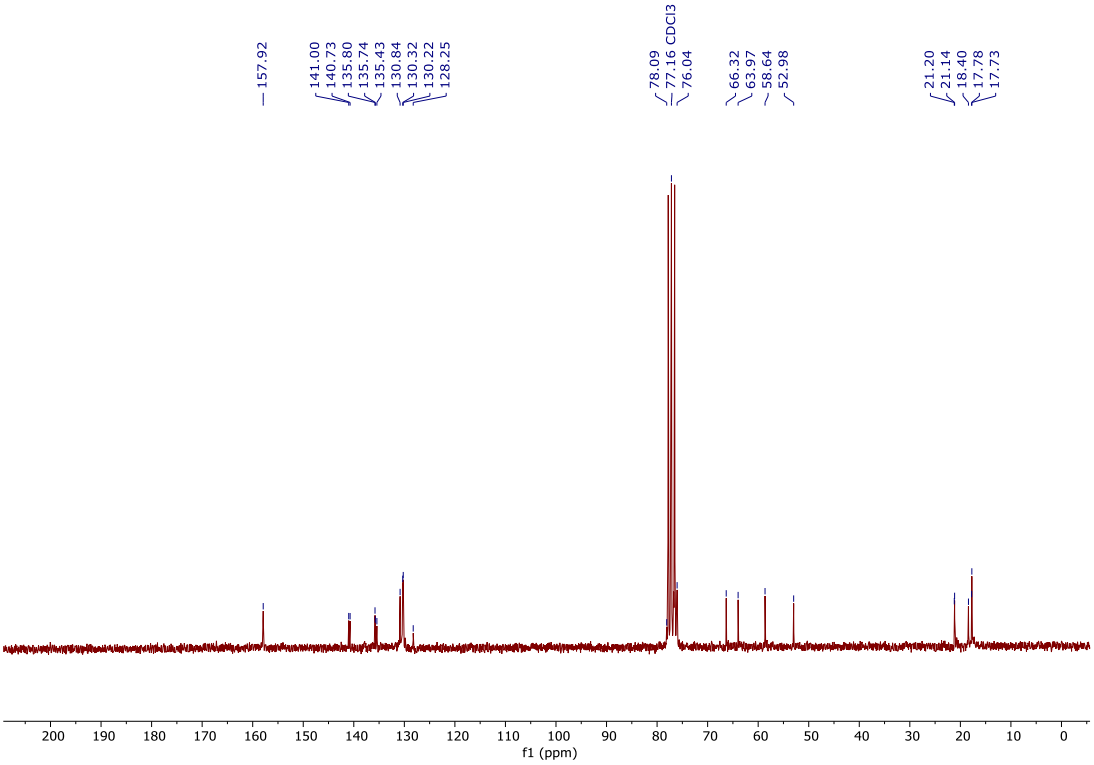

Fig. S6. ^{13}C-NMR spectrum of compound **3.**

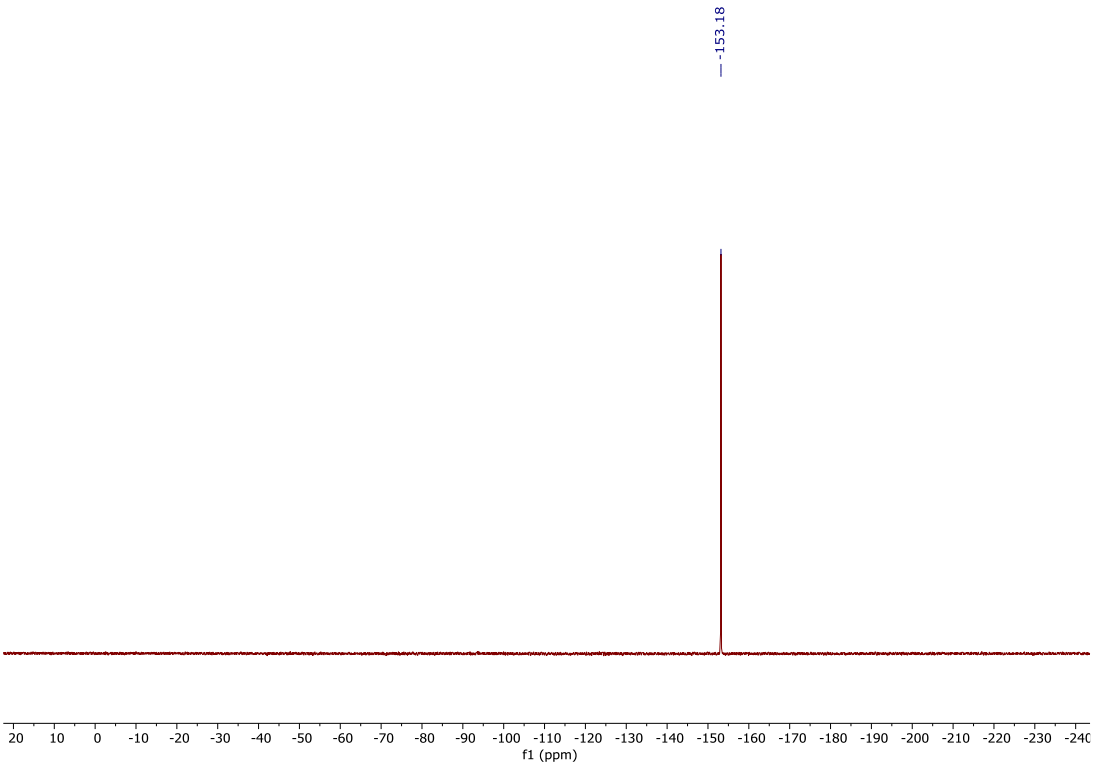

Fig. S7. ^{19}F-NMR spectrum of compound **3**.

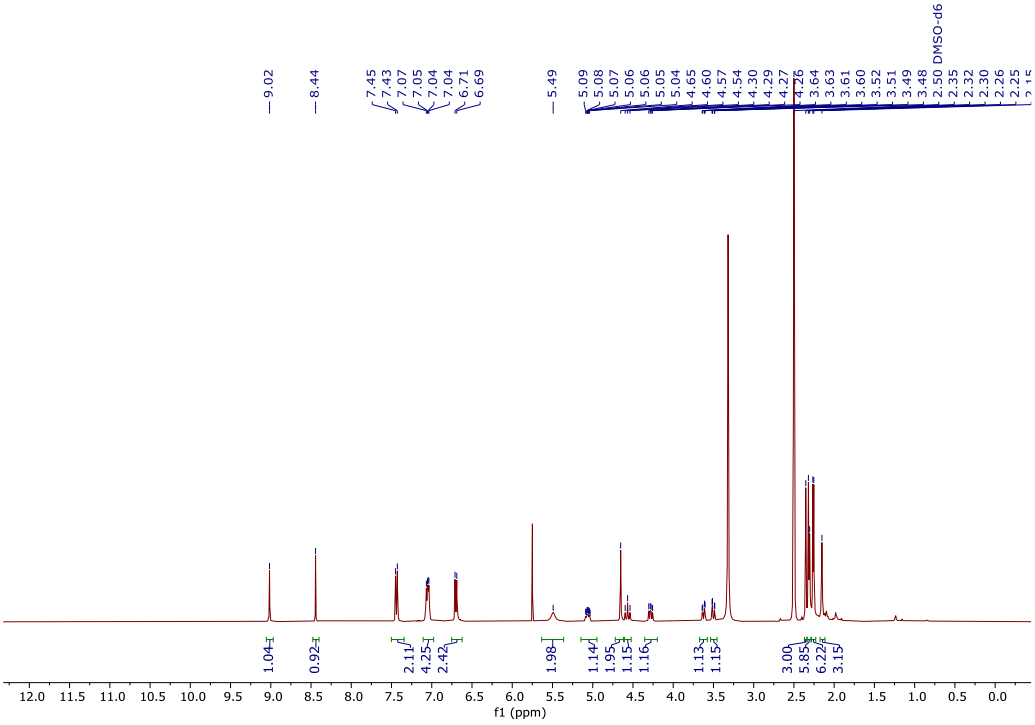

Fig. S8. ^{1}H-NMR spectrum of compound **5.**

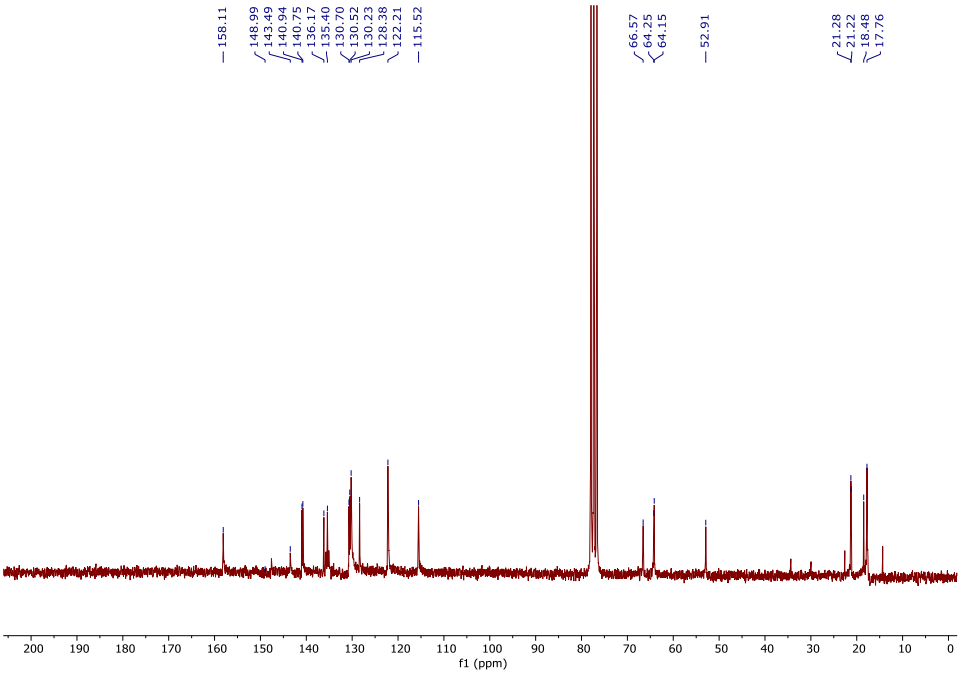

Fig. S9. ^{13}C-NMR spectrum of compound **5.**

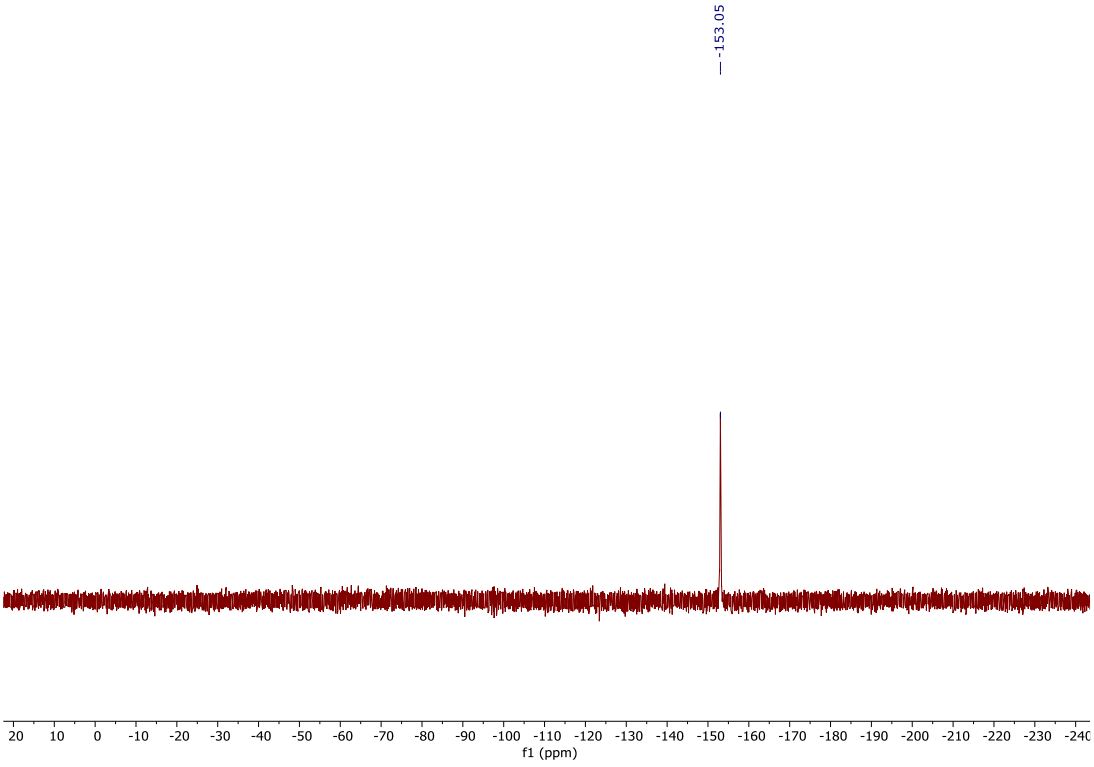

Fig. S10. ^{19}F-NMR spectrum of compound **5.**

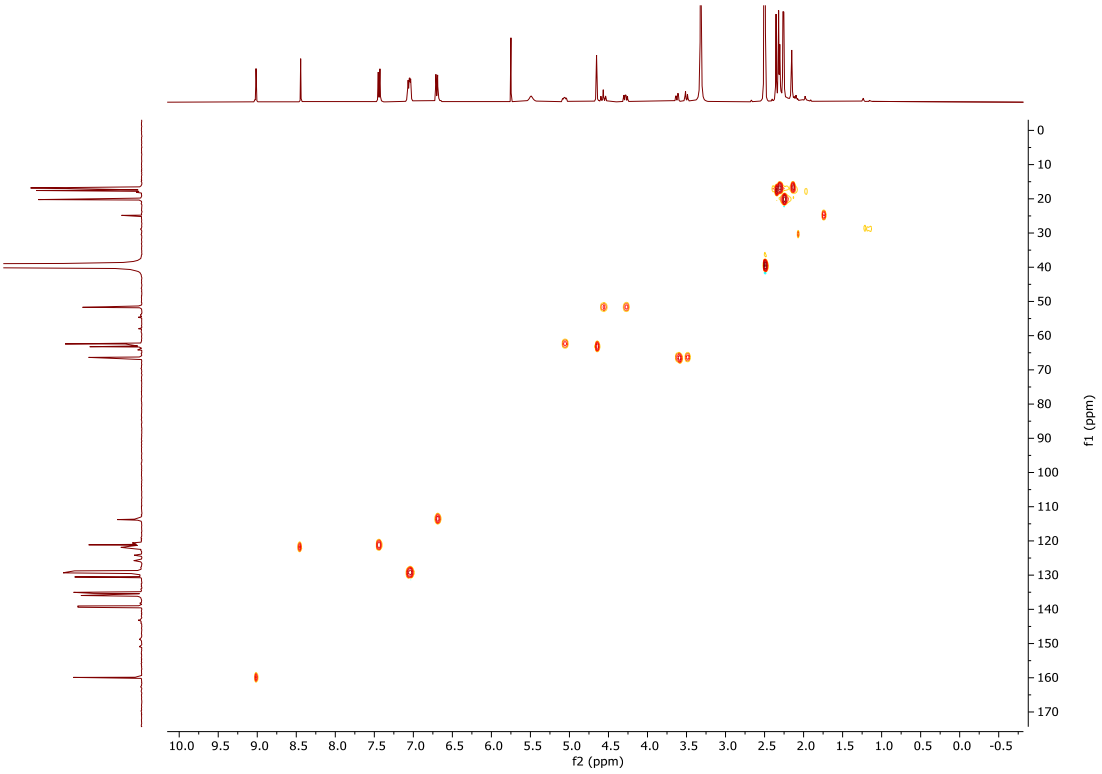

Fig. S11. ^{1}H, ^{13}C-HSQC NMR (500MHz, DMSO-d_6) of compound **5**.

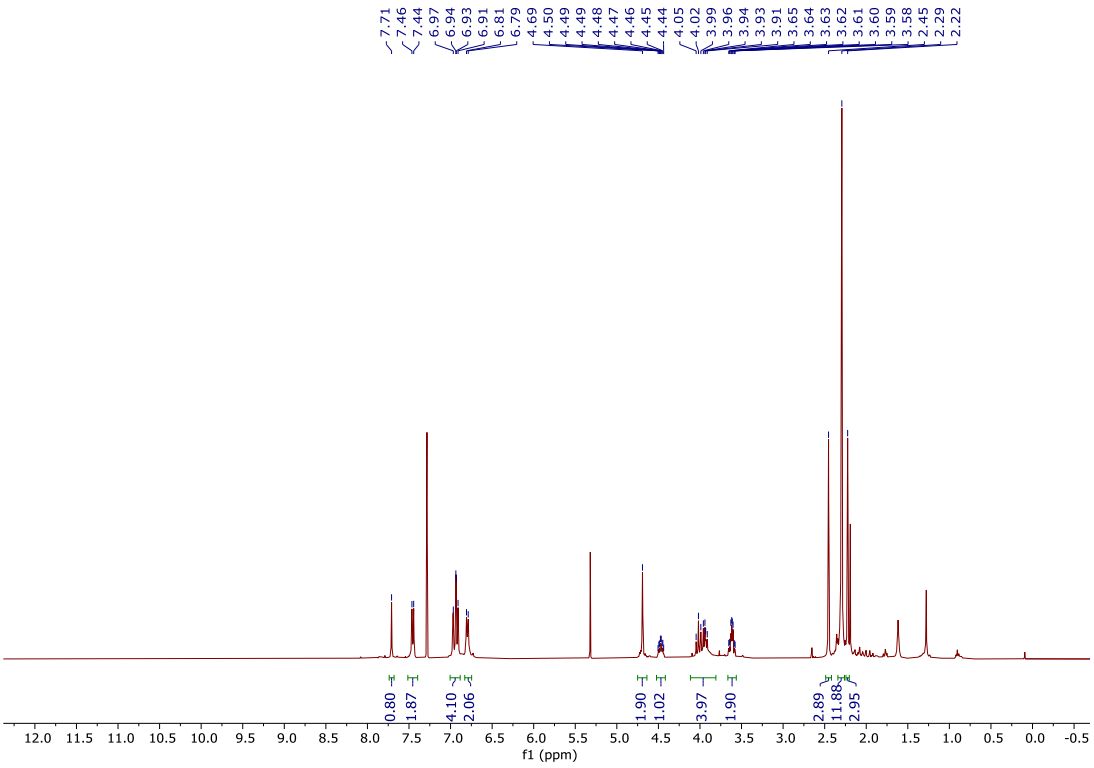

Fig. S12. ^{1}H-NMR spectrum of compound **6.**

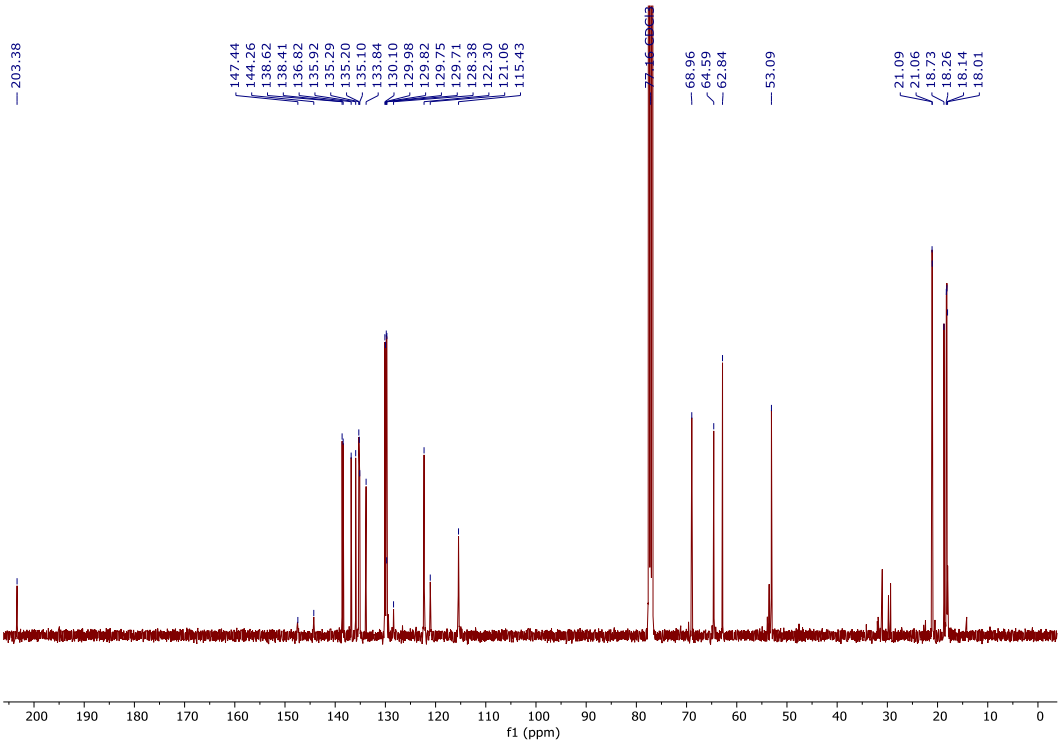

Fig. S13. ^{13}C-NMR spectrum of compound **6.**

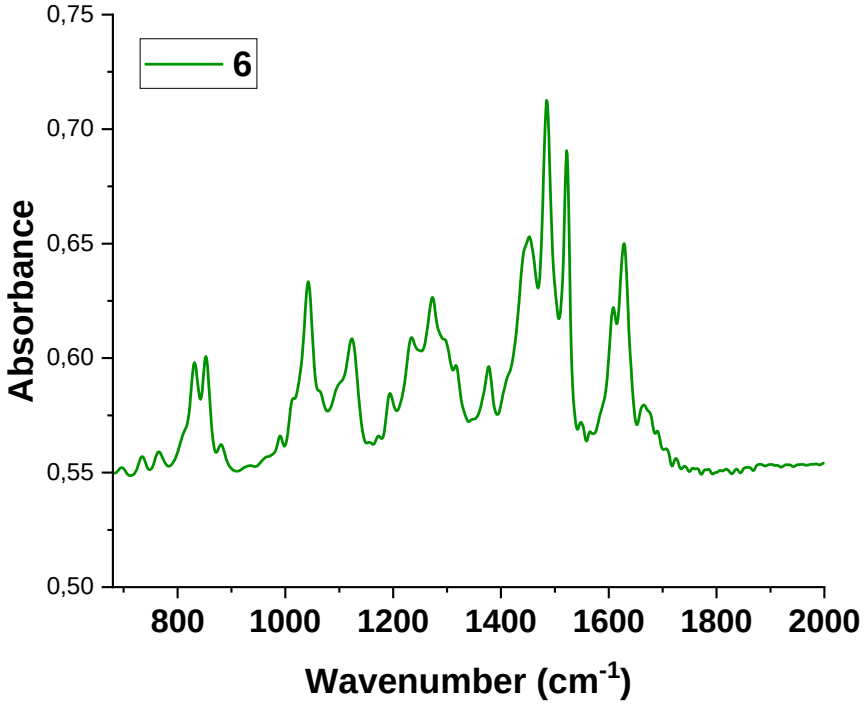

Fig. S14. FT-IR spectrum of **6**

Removal of metal residues from MWCNTs via acid treatment (7)

In a round bottom flask charged with 500 mg MWCNTs (NanoAmor, CNTs > 95%), 250 mL of concentrated HCl (36% v/v) were added. The mixture was briefly sonicated for 1 h and then was left stirring under reflux for 4h. Afterwards, it was poured into a flask containing 500 mL of ice-cold distilled water and filtered through PTFE membrane (0.2 μm pore size), followed by extensive washing with distilled water and finally with EtOH. The solid residue was dried at 90 ˚C for 10 h. 495 mg of cleaned MWNTs (with lesser metal traces) were obtained as a black amorphous powder.

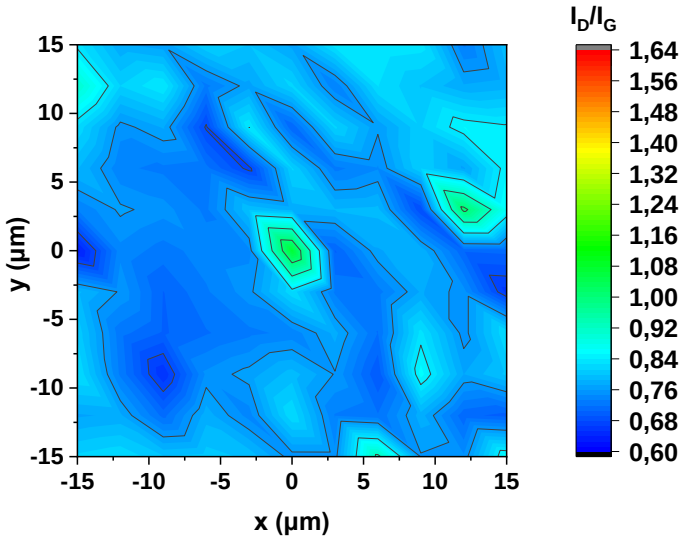

Fig. S15. Raman spectral map of **7**.

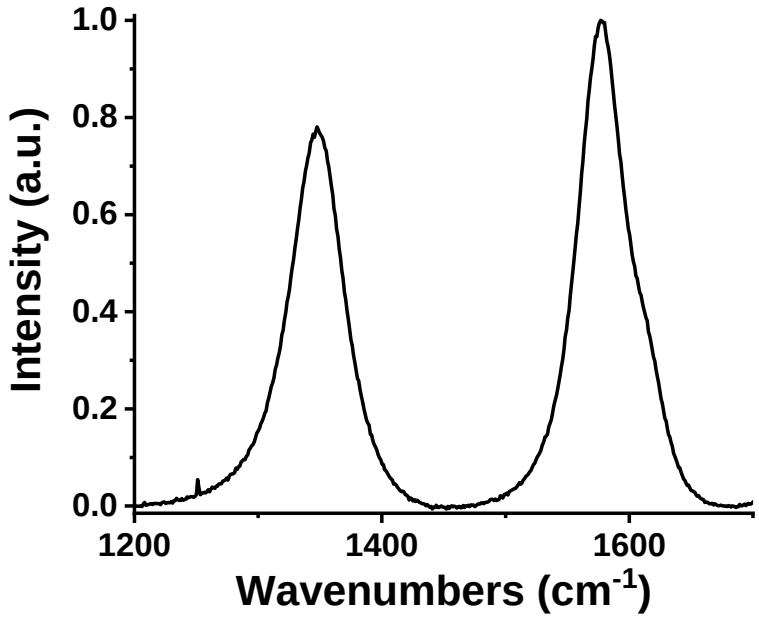

Fig. S16. Average Raman spectrum (605 measurements) focusing on D and G band region of **7** (exc. 514 nm).

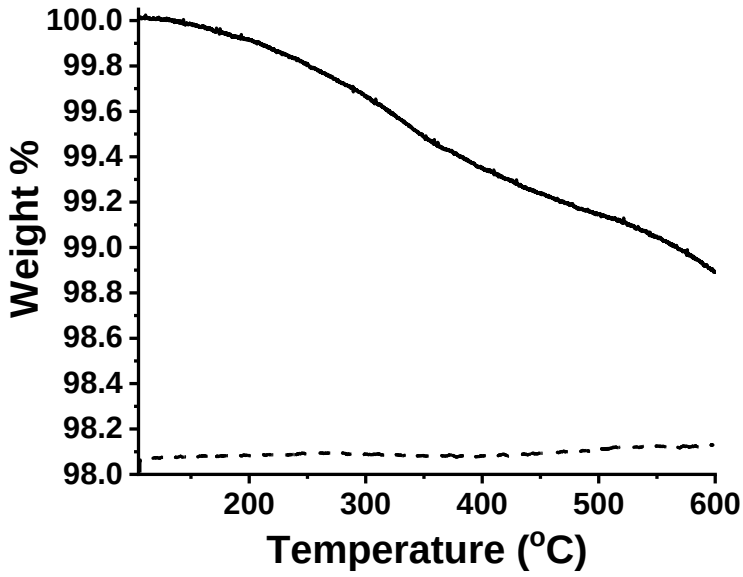

Fig. S17. TGA graph (solid line) and derivative of % weight to temperature (dashed line) of **7**.

Oxidized Multi-Walled Carbon Nanotubes 8 (oMWNTs)[S5-8]

Experimental procedure:

In a typical procedure, a thick-walled Schlenk tube is charged with 200 mg cleaned MWNTs and 48 mL of a 3:1 $^{v}/_{v}$ H_2SO_4:HNO_3 mixture. The mixture is bath sonicated for 3 h at 40 ˚C ± 5 ˚C. After dilution of the mixture with distilled water, it is filtered through PTFE membrane and washed with copious amount of distilled water until the pH is ca. 6.5-7. The solid residue is dried at 60 ˚C for 4 h and under high vacuum for several hours. 195 mg of oMWNTs are obtained as black powder.

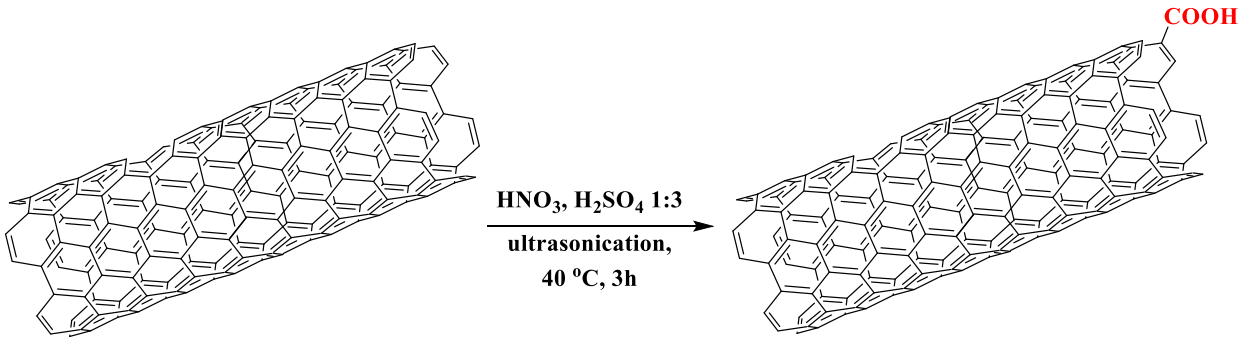

7 **8**

Scheme S1. Preparation route of oxidized MWNTs **8**.

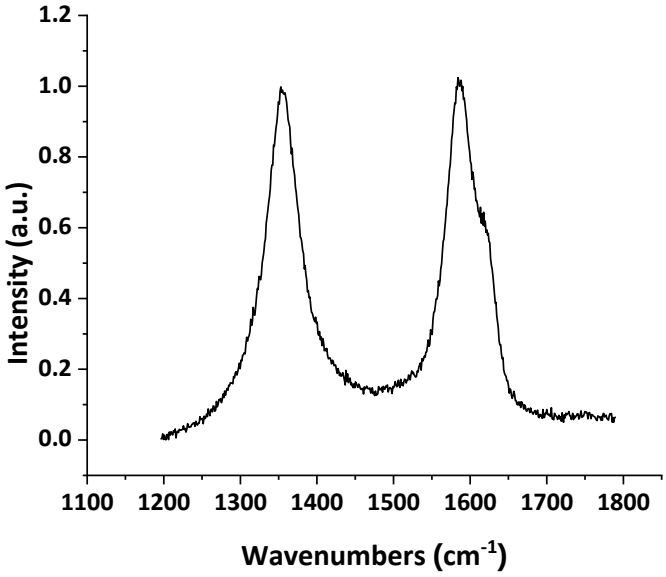

Figure S18. Average Raman spectrum (605 measurements) focusing on D and G band region of oxidized MWCNTs **8** (exc. 514 nm).

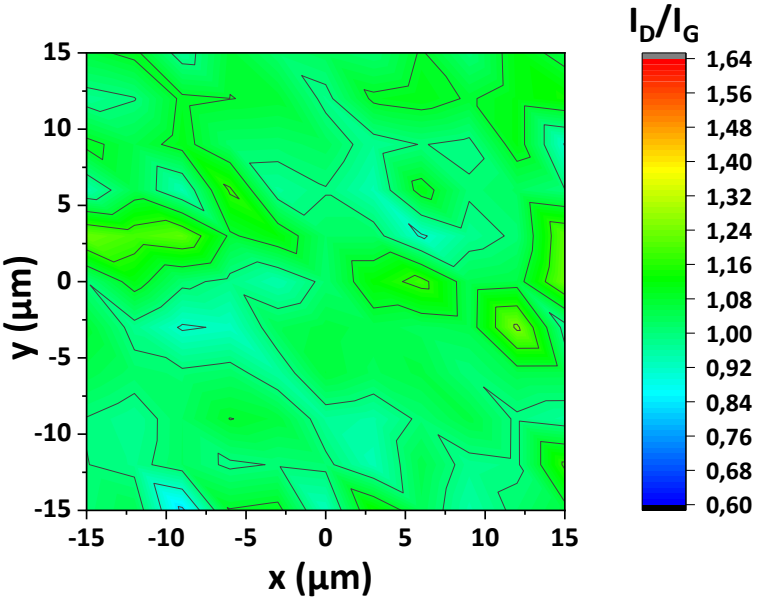

Figure S19. Raman spectral map of oxidized MWNTs **8** (exc. 514 nm).

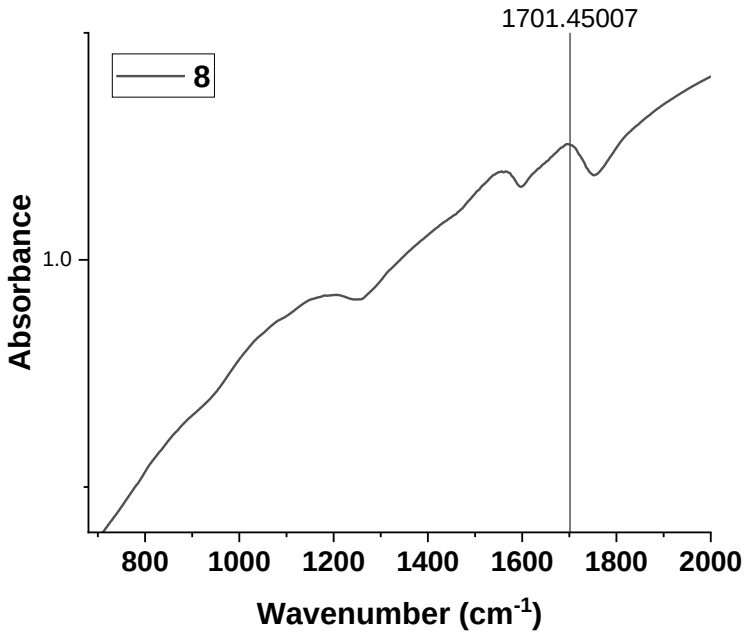

Fig. S20. ATR-FTIR spectra of **8**, which exhibits a distinct -C=O stretching vibration observed at 1702 cm^{-1}.

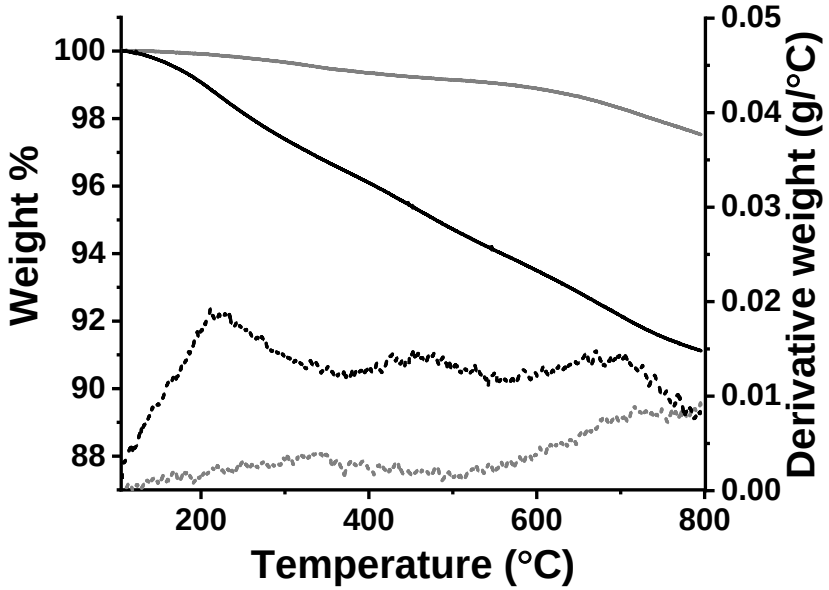

Figure S21. Thermographs (solid lines) and derivatives of weight to temperature (dashed lines) of cleaned MWNTs **7** (dark grey) and oxidized oMWNTs **8** (black). At 600 degrees loss: 6.5%, corresponding to 1 -COOH ligand per 54 C atoms of MWCNTs.

oMWNTs-CuNHC 9

Experimental procedure:

Carboxylic groups of oMWNTs are activated via reacting with $SOCl_2$ to produce carbonyl chloride groups. In a typical procedure, a fine dispersion of oMWNTs (10 mg) in $SOCl_2$ (*ca.* 1 mg mL^{-1}) is prepared with the aid of bath sonication. The mixture is left to stir under reflux overnight with a $CaCl_2$ trap attached, followed by removal of chlorinating agent *in vacuo*. Finally, the solid residue is redispersed in dry CH_2Cl_2, and the mixture is again subjected to evaporation to remove traces of $SOCl_2$. This procedure was carried out 3 times. Activated oMWNTs were collected as black solid and used in the next step without further purification.

To a dispersion of activated oMWNTs in 10 mL dry DMF (*ca.* 1 mg mL^{-1}), 3 mL of Et_3N were added and the mixture was let to stir at 0 ºC for 15 min. Next, **6** (24 mg, 0,04 mmol, 40 eq.) were added and the mixture was left for another 15 min. at 0 ºC. Then, the mixture is left to attain R.T. and is finally heated to 70 ºC for 72 h. After filtration through PTFE membrane and consequent washes with DMF, $CHCl_3$ and EtOH, the solid residue was dried at 60 ºC under high vacuum overnight to afford 10 mg of **9** as a black solid.

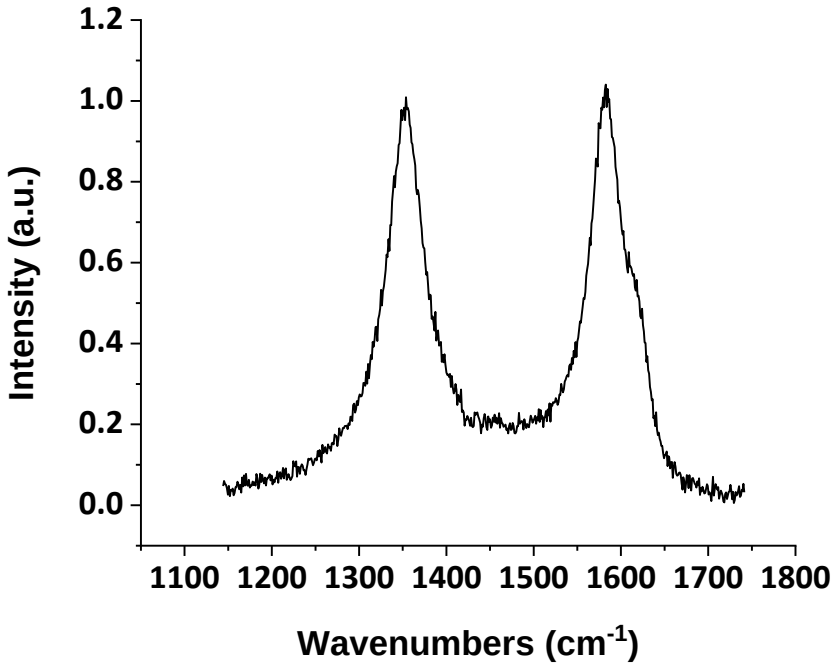

Figure S22. Average Raman spectrum (605 measurements) focusing on D and G band region of **9** (exc. 514 nm).

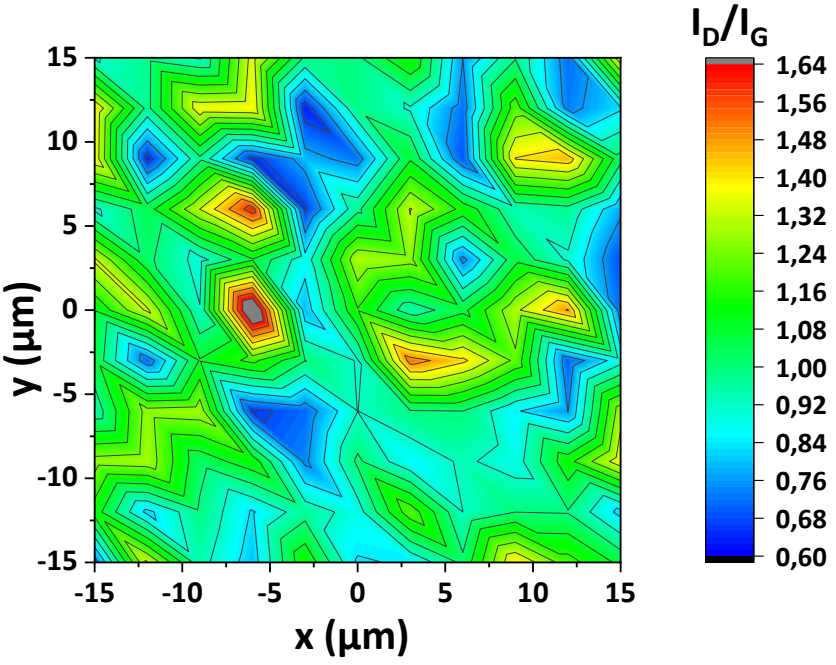

Figure S23. Raman spectral map of **9** (exc. 514 nm).

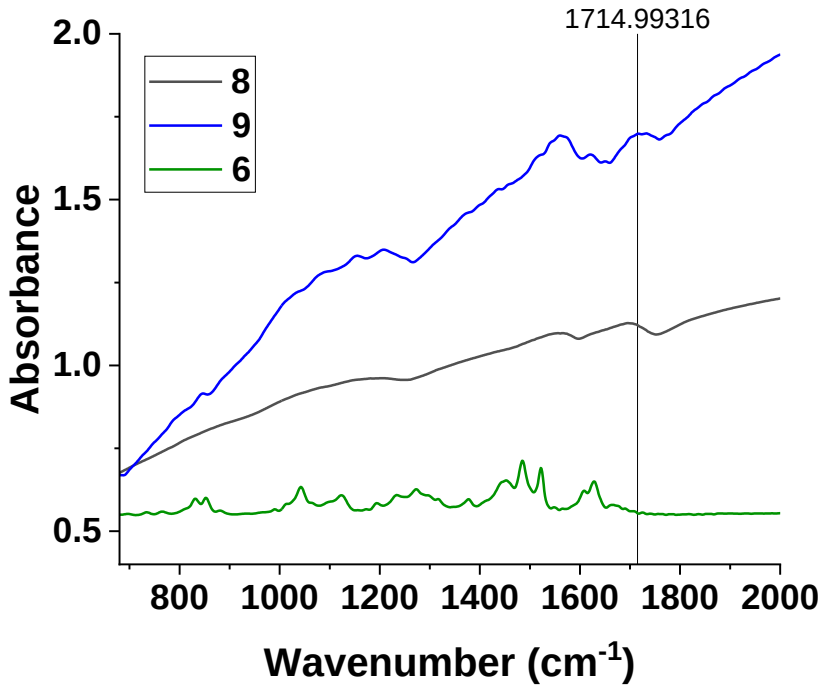

Fig. S24. ATR-FTIR spectra of **6** (green), **8** (black) and **9** (blue) which exhibits the characteristic fingerprint bands of **6**, alongside a prominent -C=O stretching vibration observed at 1715 cm^{-1}.

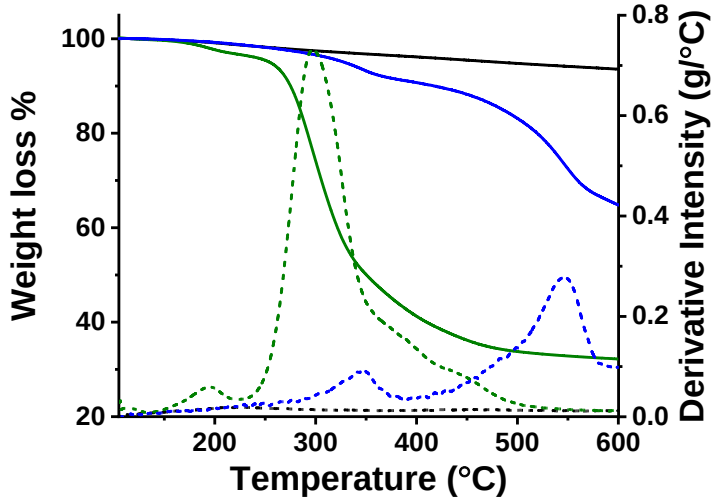

Figure S25. TGA graphs (solid lines) and derivatives of % weight to temperature (dashed lines) of **8** (black), **9** (blue) and **6** (green).

XPS of 9

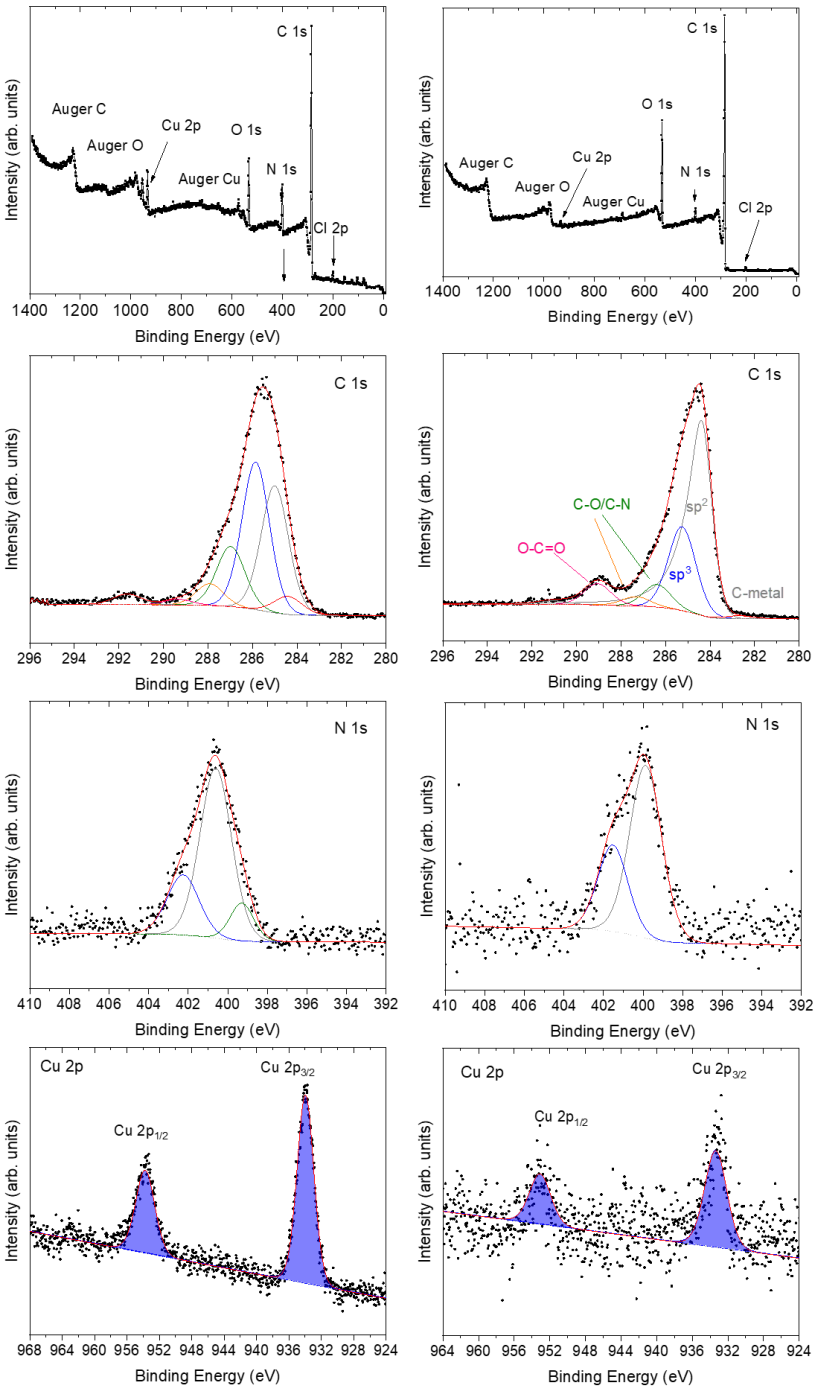

Figure S26. Survey and narrow scans of C 1s, N 1s and Cu 2p for complex **6** (left panel) and nanomaterial **9** (right panel).

Advanced electrocatalyst 10

Experimental procedure:

To a sonicated (5 min.) and degassed (5 min.) dispersion of **9** (6 mg) in 3,5 mL H_2O and 4,5 mL EtOH mixture, $NiCl_2.6H_2O$ (0,7 mg, 0.003 mmol) in 1 mL H_2O was added dropwise under vigorous stirring. The mixture was briefly sonicated and left to stir vigorously under N_2 for 15 min. $NaBH_4$ (2.3 mg, 0.06 mmol) was then added and the mixture was left to stir vigorously for 10 h under N_2. Removal of impurities was carried out via two-fold dilution with H_2O:EtOH (1:1), centrifugation (4,000 rpm, 20 min) and three cycles of redispersion and centrifugation of precipitate, twice in 27 mL H_2O:EtOH (1:1) and once only in EtOH (9 mL). The solid residue was dried under N_2 stream and at 80 ˚C overnight. 6 mg of black solid was finally collected.

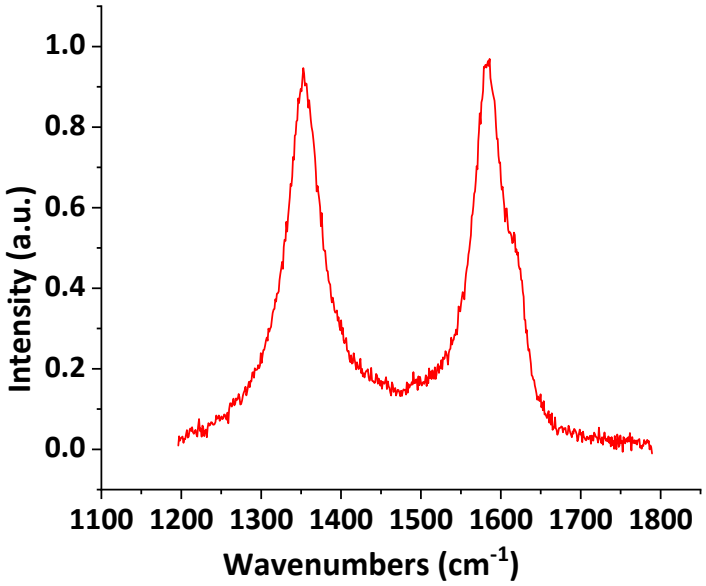

Figure S27. Average Raman spectrum (605 measurements) focusing on D and G band region of **10** (exc. 514 nm).

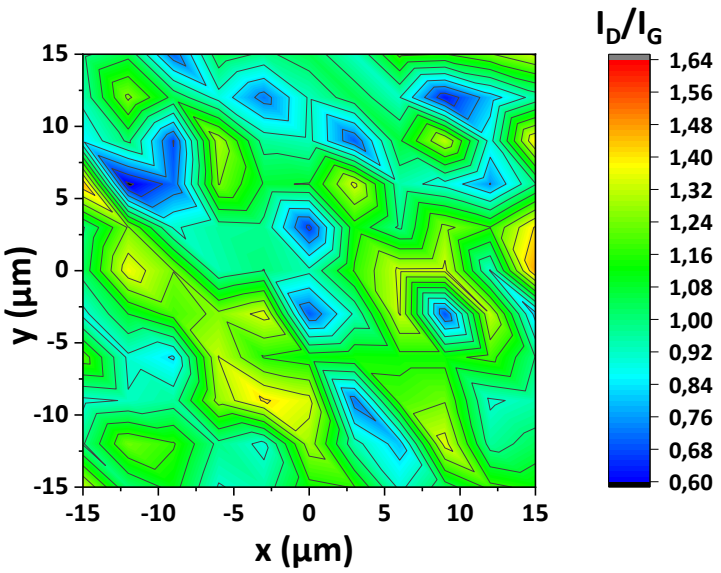

Figure S28. Raman spectral map of **10** (exc. 514 nm laser line).

Nanomaterial	I_D/I_G ratio[a]	G shift (cm^{-1})[b]	D shift (cm^{-1})[b]
7	0.80	1577	1348
8	1.03	1587	1355
9	1.02	1583	1353
10	1.03	1583	1353

Table S1. [a]I_D/I_G average ratio (error bar = ± 0.01) [b]G and D band average position for nanomaterials **7**-**10** (error bar = ± 1 cm^{-1}).

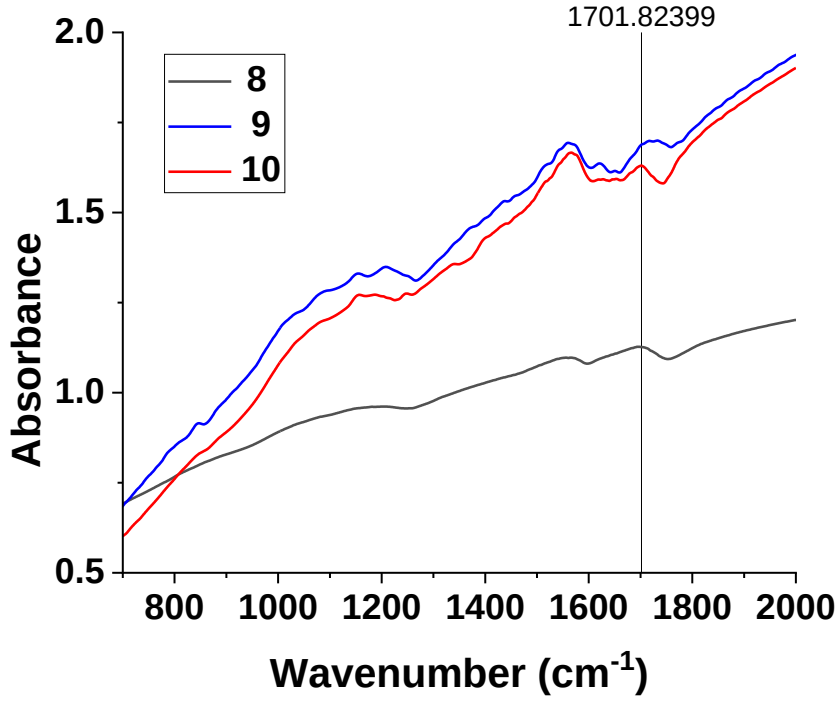

Fig. S29. ATR-FTIR spectra of **8** (black), **9** (blue) and **10** (red).

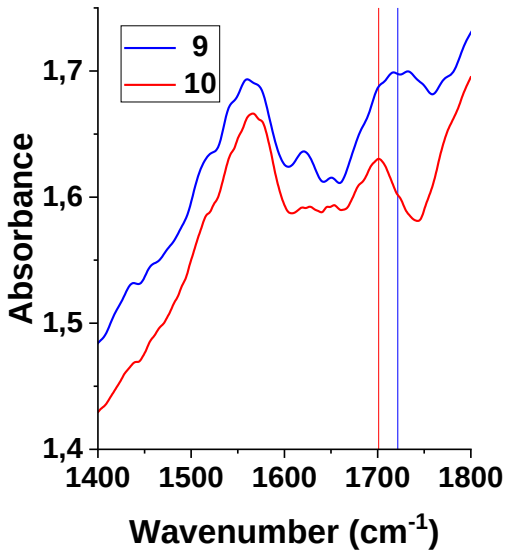

Fig. S30. ATR-FTIR spectra of **9** (blue) and **10** (red) focusing on the amide -C=O region, revealing a 13 cm^{-1} shift to lower wavenumbers for **10**, indicating a change in the electronic environment due to interaction with NiNCs.

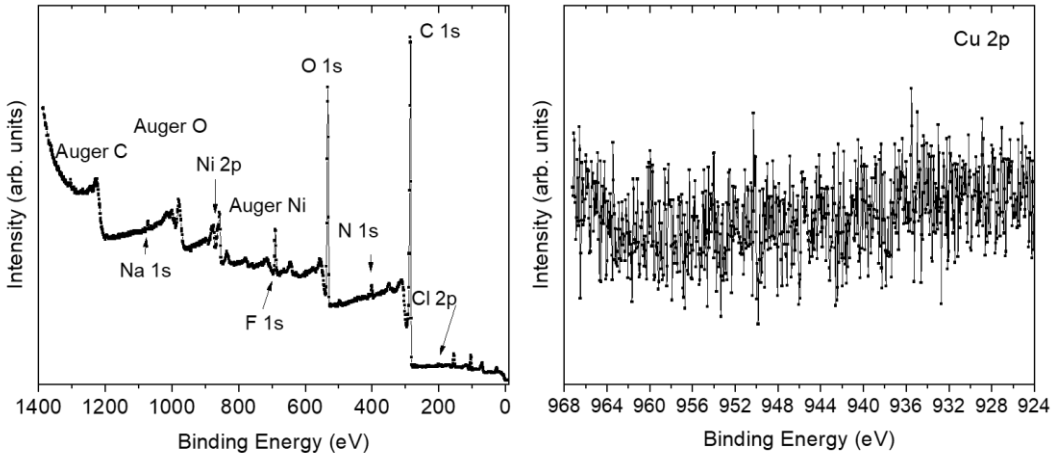

Fig. S31. Survey scan and narrow Cu 2p scan of **10**.

C1s assignment	**9**	**10**
Ni-*C*-N-	-	282.7
***C*sp2**	284.4 eV	284.4 eV
***C*sp3**	285.3 eV	285.3 eV
***C*-N**	286.4 eV	286.4 eV
C*-O-*C	287.3 eV	287.3 eV
adsorbed CO_2 / Oxidized carbon	289.1 eV	289.1 eV
π-π* shake-up satellite	291.0 eV	291.0 eV
N1s assignment	**9**	**10**
Ni-C-*N*-	-	399.2
-*N*-N=*N*- (trz)	400.0 eV	400.2 eV
-N-*N*=N- (trz)	401.4 eV	401.8 eV

Table S2. Comparative XPS narrow scans of C 1s and N 1s of nanomaterials **9** and **10**.

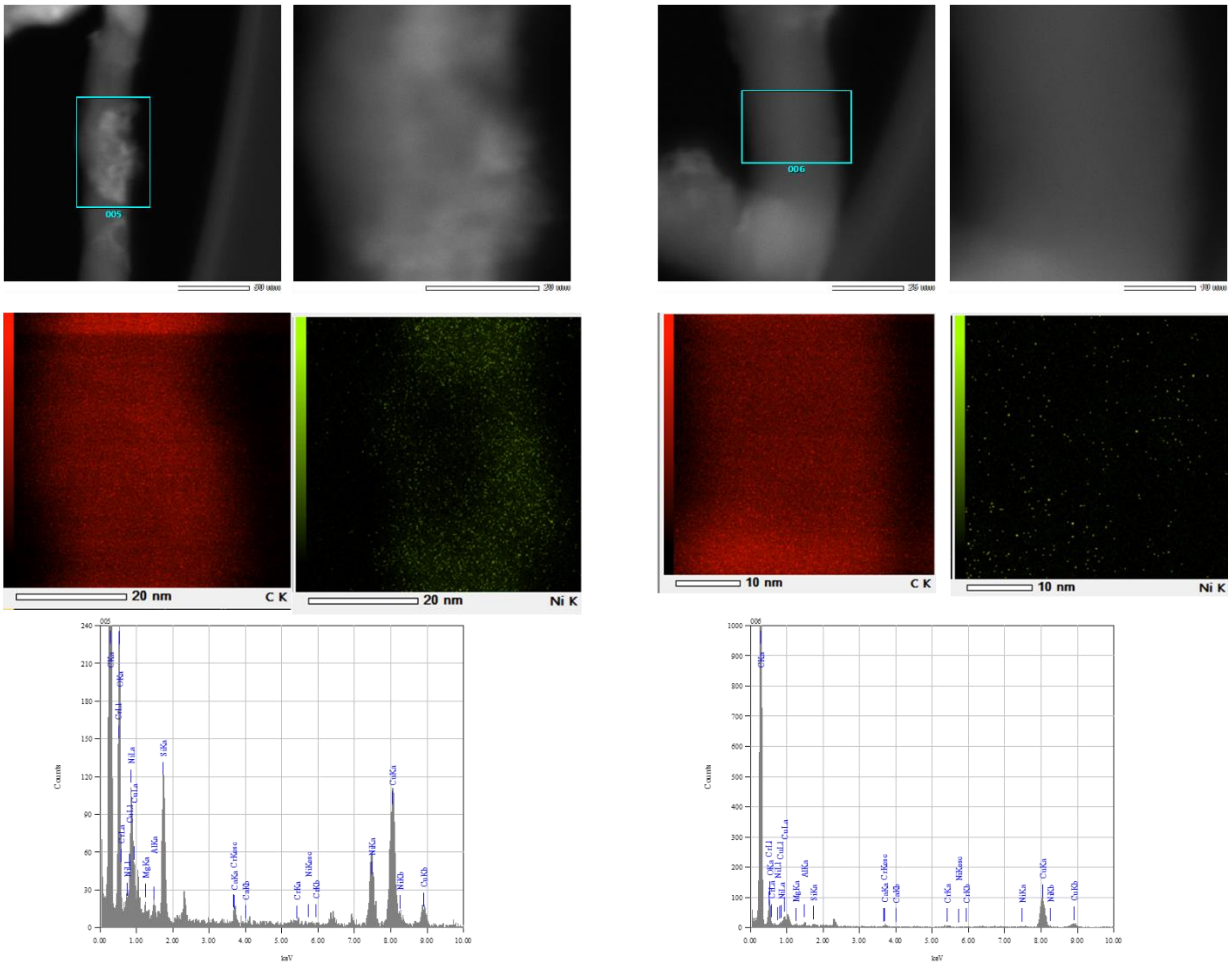

Fig. S32. HAADF-STEM images and EDS mapping on NiNCs area (left panel) and MWCNTs area (right panel) in **10**.

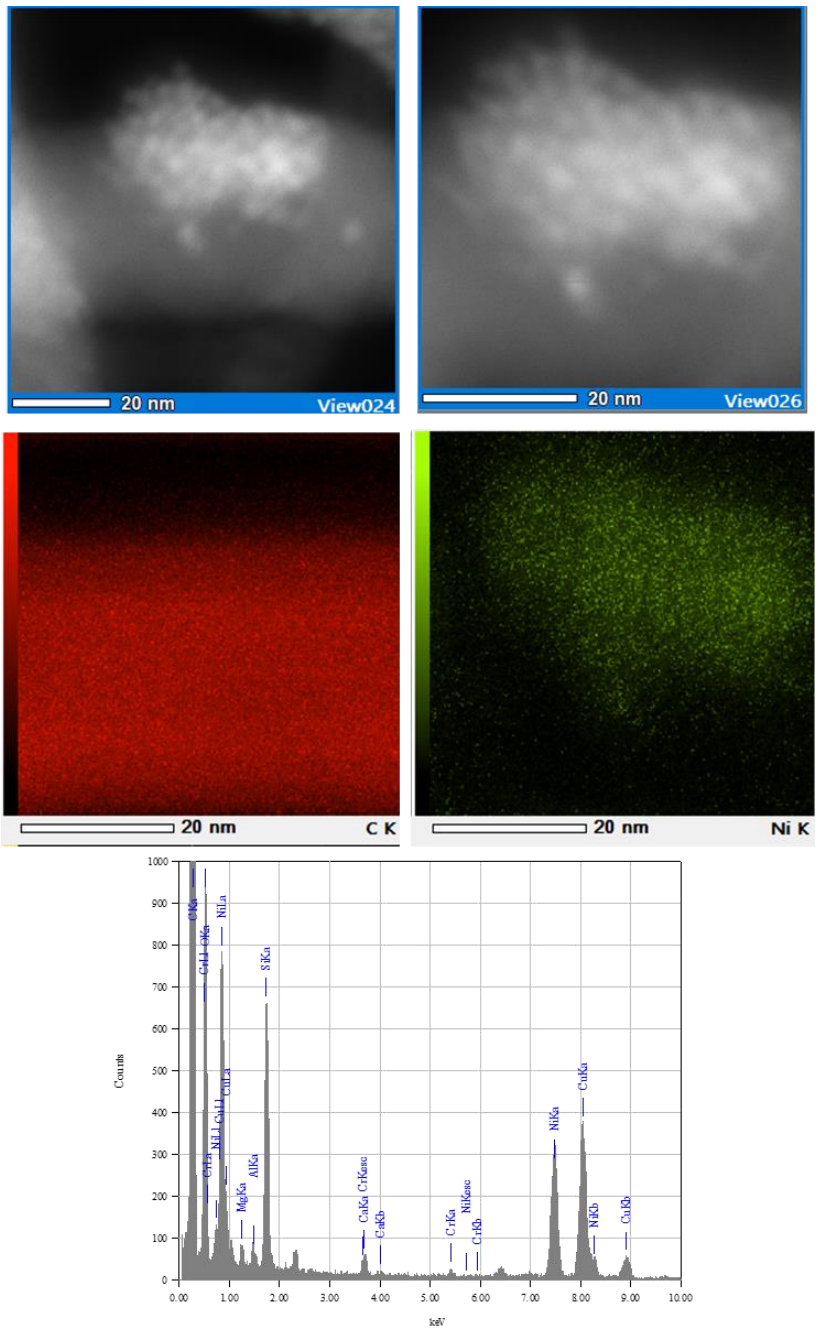

Fig. S33. HAADF-STEM images and EDS mapping of MWCNTs with NiNCs in **10**.

Calculation of n_{Ni} electroactive sites before and after activation for 10.

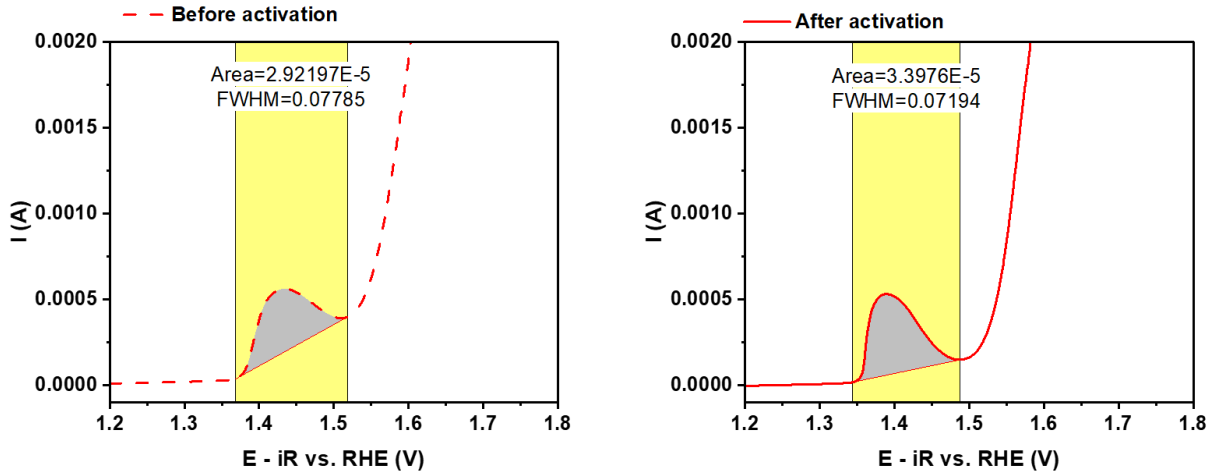

Fig. S34. Integration of the anodic $Ni^{II/III}$ before and after activation.

Note S.1. Calculations for number of electrons transferred

Faraday's Law:

Q = n.F,

where Q is the total charge,

n is the number of electrons transferred (n = 1)

F is Faraday's constant (96,485 C/mol)

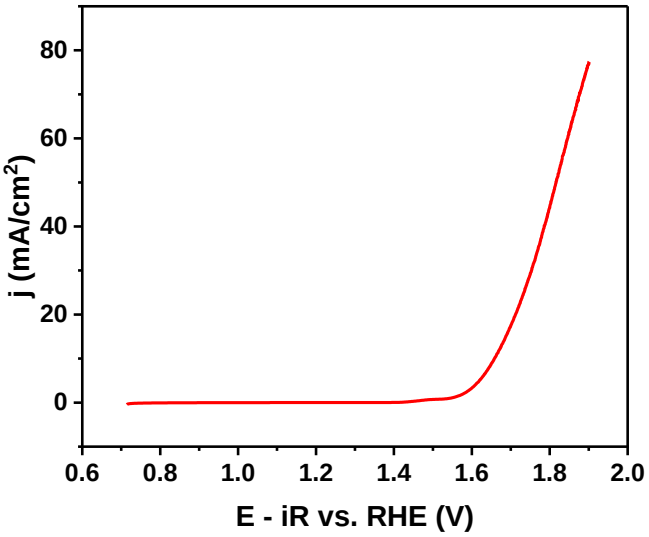

Fig. S35. LSV polarization curve of **10** obtained at 1600 rpm rotation speed and 5 mV s^{-1} scan rate in 0.1M KOH up to j = 80 mA/cm^2.

Calculation of n_{Ni} electroactive sites after 10^4 OER cycles for 10.

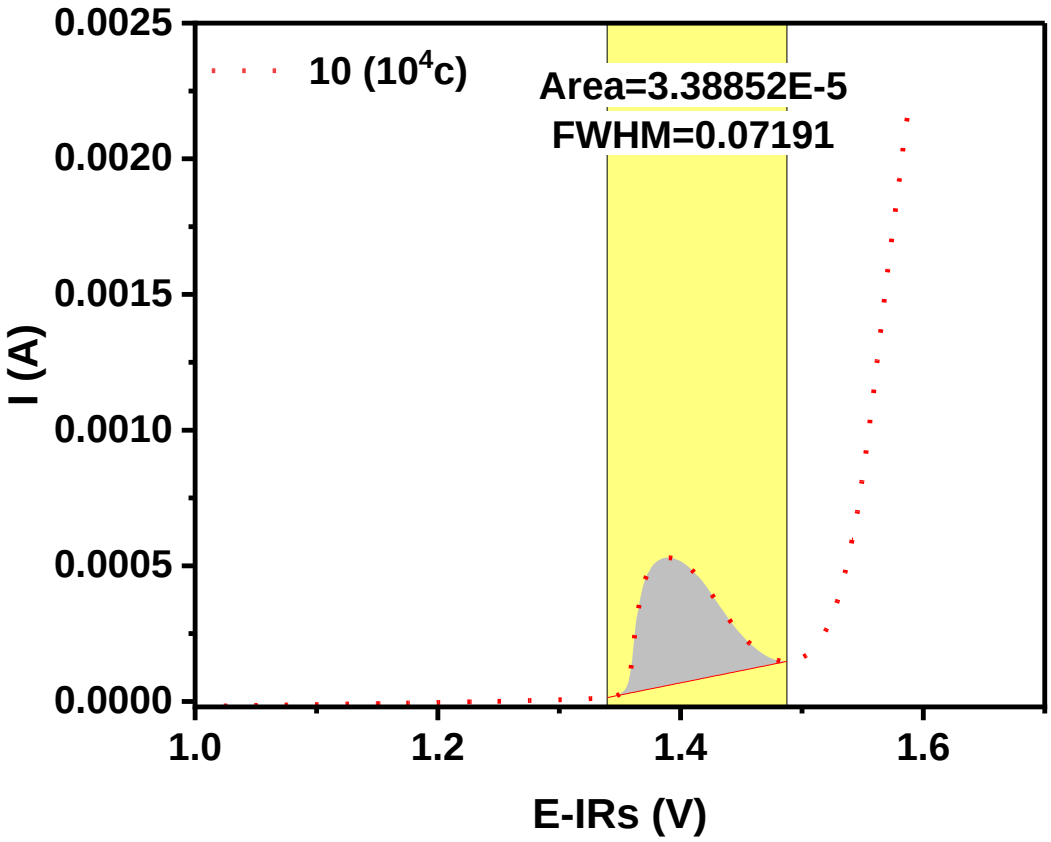

Fig. S36. Integration of the anodic $Ni^{II/III}$ after 10^4 OER cycles.

Batch	η@10 mA/cm^2 (mV)	Standard Deviation (mV)	Cycles to stabilization
1	348	±5	300
2	352	±7	1000
3	349	±6	1200
4	350	±6	2000
5	351	±5	1500

Table S3. Summary of electrocatalyst **10** performance across five independent synthetic batches in 0.1 M KOH.

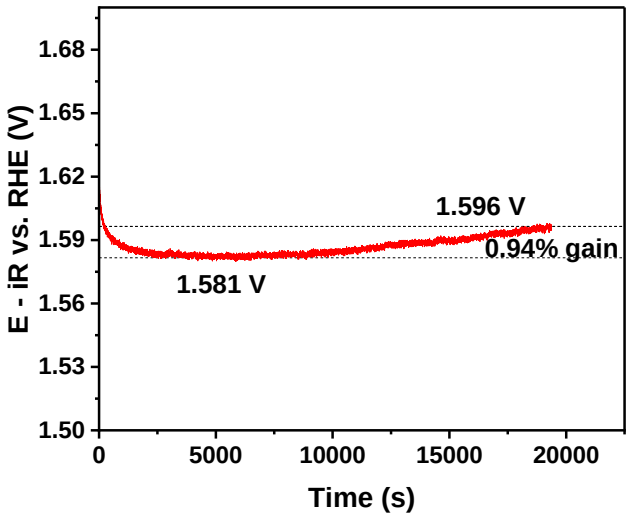

Fig. S37. Long-term potentiometry in 0.1M KOH for over 5 hours at 10 mA/cm^2, showing a minimal gain of 15 mV in overpotential, corresponding to a 0.94% increase.

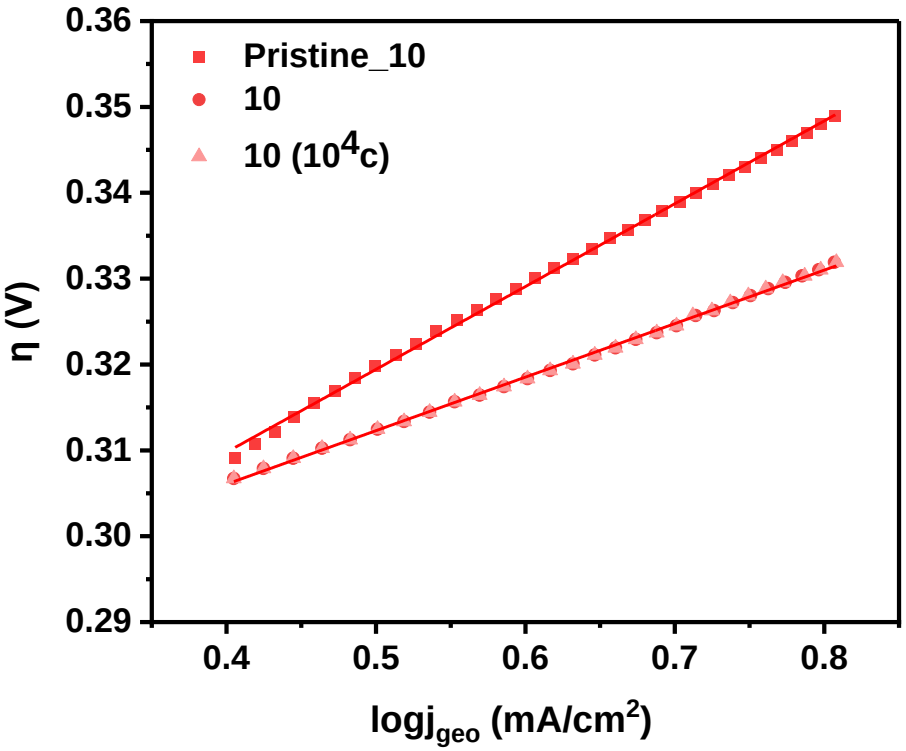

Fig. S38. Tafel slopes for pristine **10**, **10** (after activation) and **10** after 10^4c.

Note S.2. Calculations for exchange current density j0

Tafel Equation:

$\eta = b \cdot \log j + \alpha$

where:

η: overpotential (mV)

j: current density (mA/cm^2)

b: Tafel slope (mV/dec)

α: intercept of the linear Tafel fit

The j0 was calculated assuming η = 0 when j = j0.

Double-layer capacitance (C_{dl}) measurements for nanomaterials 8, 9, electrocatalyst 10 and commercial RuO_2.

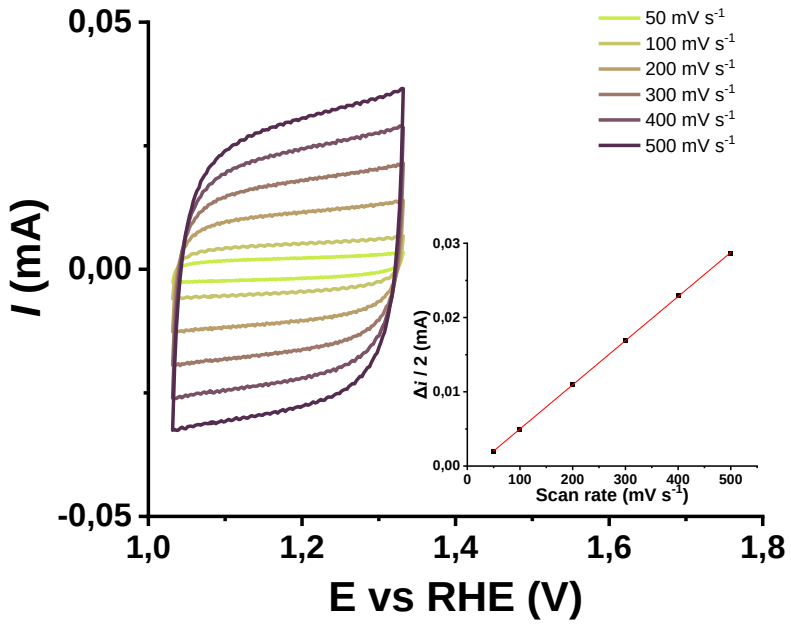

Fig. S39. Cyclic voltammograms of **8** at scan rates 50-500 mV s^{-1} (Inset: Δi/2 vs scan rate for C_{dl} calculation) in N_2-saturated 0.1 M KOH electrolyte.

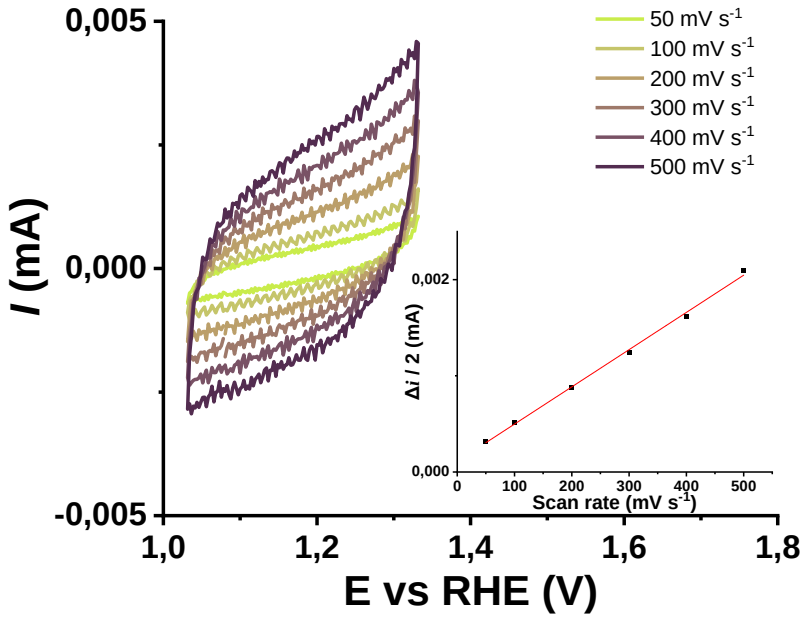

Fig. S40. Cyclic voltammograms of **9** at scan rates 50-500 mV s^{-1} (Inset: Δi/2 vs scan rate for $\mathbf{C_{dl}}$ calculation) in N_2-saturated 0.1 M KOH electrolyte.

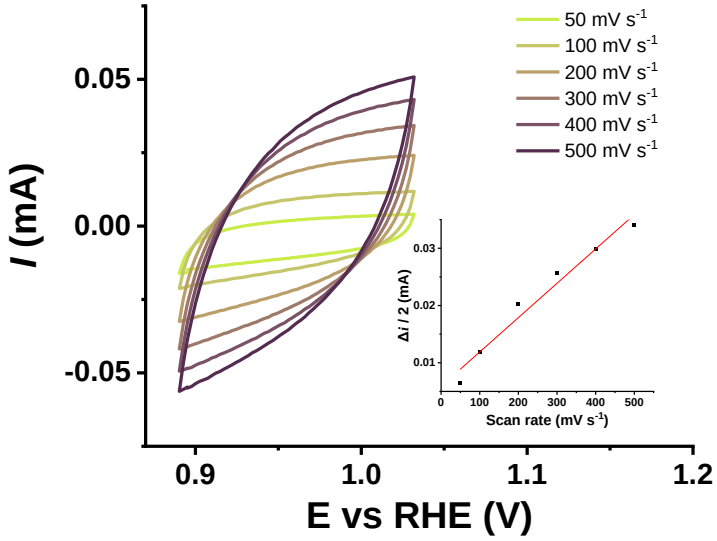

Fig. S41. Cyclic voltammograms of **10** at scan rates 50-500 mV s^{-1} (Inset: Δi/2 vs scan rate for $\mathbf{C_{dl}}$ calculation) in N_2-saturated 0.1 M KOH electrolyte.

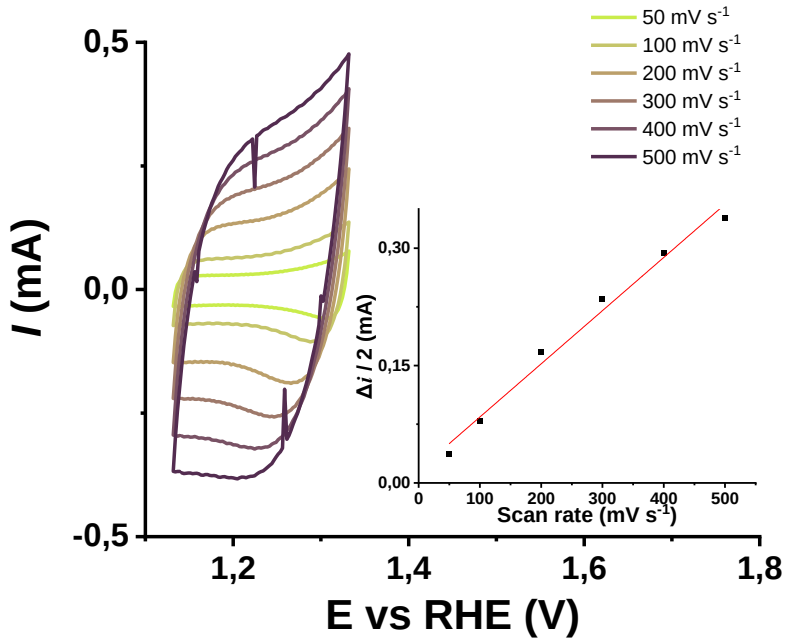

Fig. S42. Cyclic voltammograms of **RuO_2** at scan rates 50-500 mV s^{-1} (Inset: Δi/2 vs scan rate for **C_{dl}** calculation) in N_2-saturated 0.1 M KOH electrolyte.

material	**Cdl**	**ESCA**
oMWCNTs 8	59.4 ± 0.2 μF	1.49 ± 0.01 cm^2
9	3.9 ± 0.1 μF	0.097 ± 0.002 cm^2
10	60.0 ± 5.5 μF	1.50 ± 0.14 cm^2
RuO_2	679.5 ± 40.9 μF	17.0 ± 1.0 cm^2

Table S4. Cdl and ESCA collective values for **10**, **8** and **RuO_2**.

Specific activity of 10, 8 and RuO_2

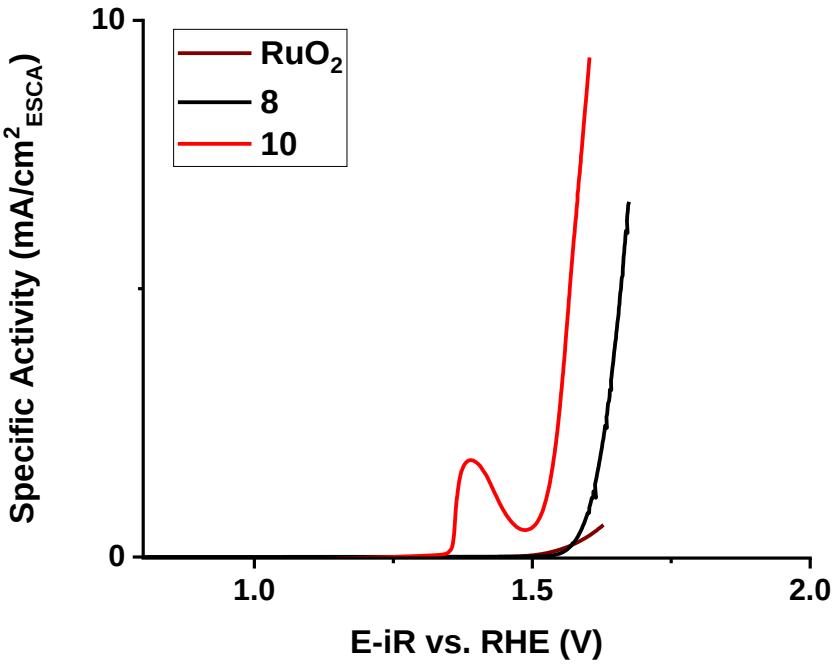

Fig. S43. Specific activity j_{ESCA} of **10**, **8** and **RuO_2**.

Intrinsic activity of 10

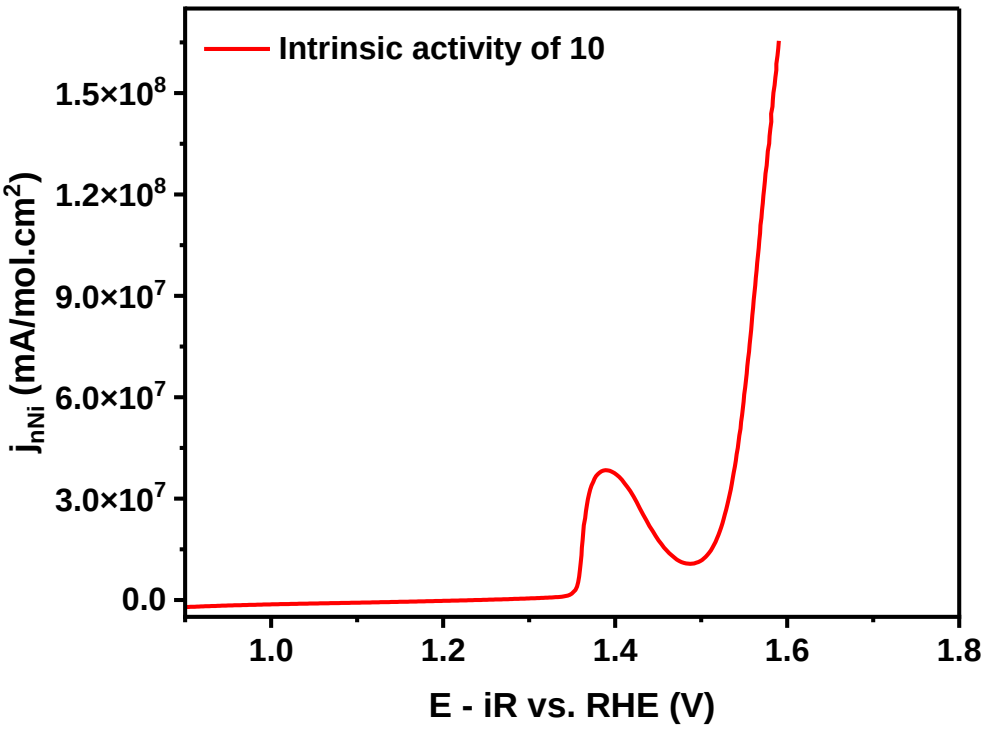

Fig. S44. Intrinsic activity j_{nNi} of **10**.

Note S.3. Calculations for TOF (s^{-1})

$$TOF = \frac{j}{n \cdot z \cdot F}$$

where:

- *j*: current density (A/cm^2),
- *n*: moles of active sites (mol),
- *z*: number of electrons transferred
- *F*: Faraday constant

Note S.4. Calculations for slope of log(TOF)-η

$$\eta = b \cdot \log(j) + \alpha$$

$$Slope = \frac{1}{b}$$

Fitted Parameters	10	8	RuO_2
Rs (Solution Resistance, Ω)	47	58	58
Rct (Charge Transfer Resistance, Ω)	55	133	114
Y0 (Constant Phase Element)	2.34 **$mS \cdot s^N$**	67.1 **$\mu S \cdot s^N$**	978 **$\mu S \cdot s^N$**
N (exponent)	0.4	0.8	0.8

Table S5. Fitted with Randles circuit (CPE) parameters of Nyquist plots. The EIS experiments were performed at j = 2-3 mA/cm^2 for **10**, **8** and **RuO_2** in 0.1M KOH.

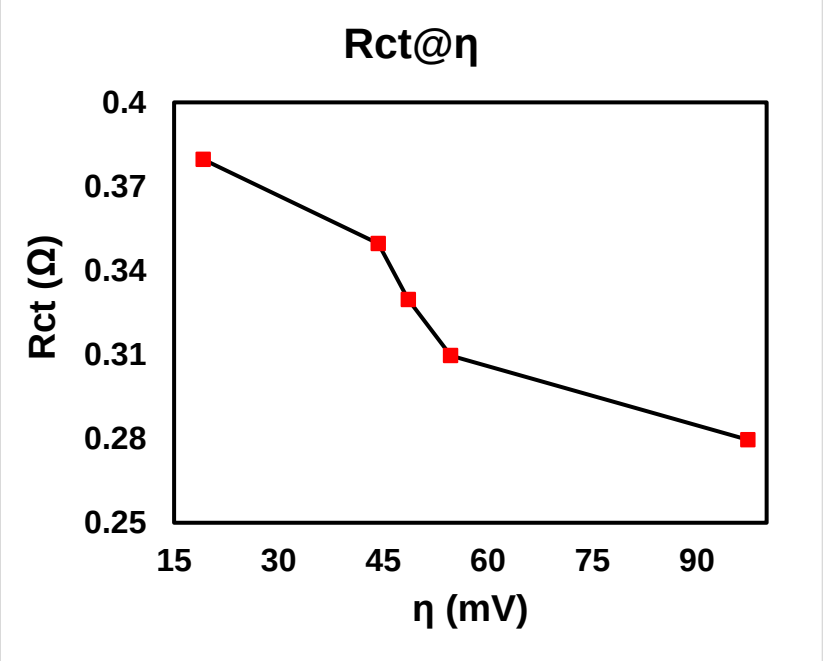

Fig. S45. Charge transfer resistance (Rct, Ω) plotted as a function of overpotential (η, mV) in the kinetic region for electrode **10**.

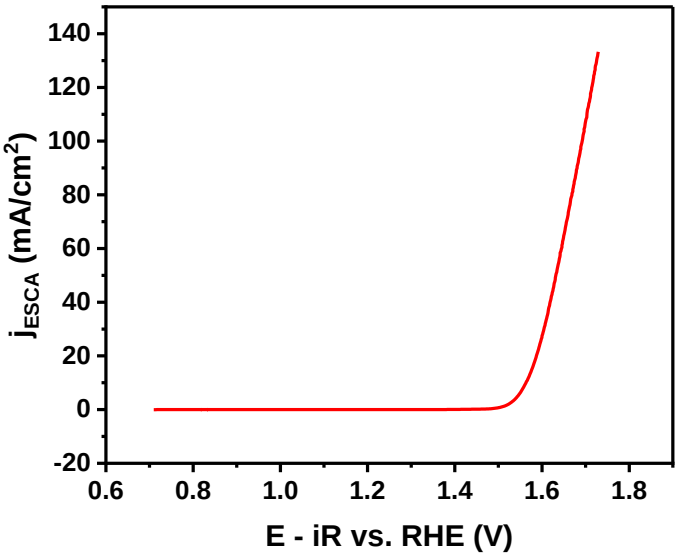

Fig. S46. Specific activity of **10** in 1M KOH at higher currents (up to j = 200 mA/cm^2).

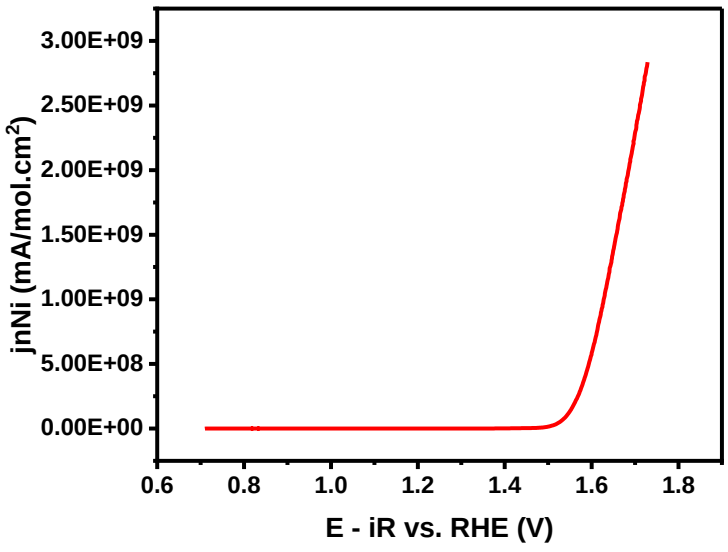

Fig. S47. Intrinsic activity of **10** in 1M KOH at higher currents (up to j = 200 mA/cm^2).

Fitted Parameters of 10	$E_{1.25}$ = 1.51 V	$E_{2.50}$ = 1.52 V	E_5 = 1.53 V	E_{10} = 1.55 V	E_{20} = 1.57 V
Rs (Solution Resistance, Ω)	7.5	7.5	7.5	7.4	7.3
Rct (Charge Transfer Resistance, Ω)	66	44.6	28.3	12.4	9.7
Cdl	51.0 µF	48.8 µF	45.7 µF	39.1 µF	35.6 µF

Table S6. Fitted with Randles circuit (Cdl) parameters of Nyquist plots of **10** across various overpotentials in 1M KOH.

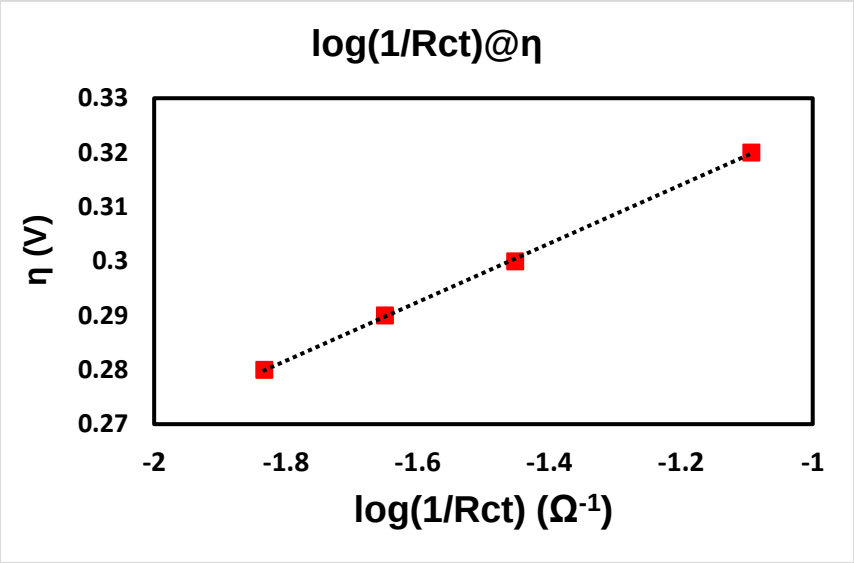

Fig. S48. Plot of log(1/Rct) in Ω^{-1} in function of η in V. Slope = 54 mV/dec.

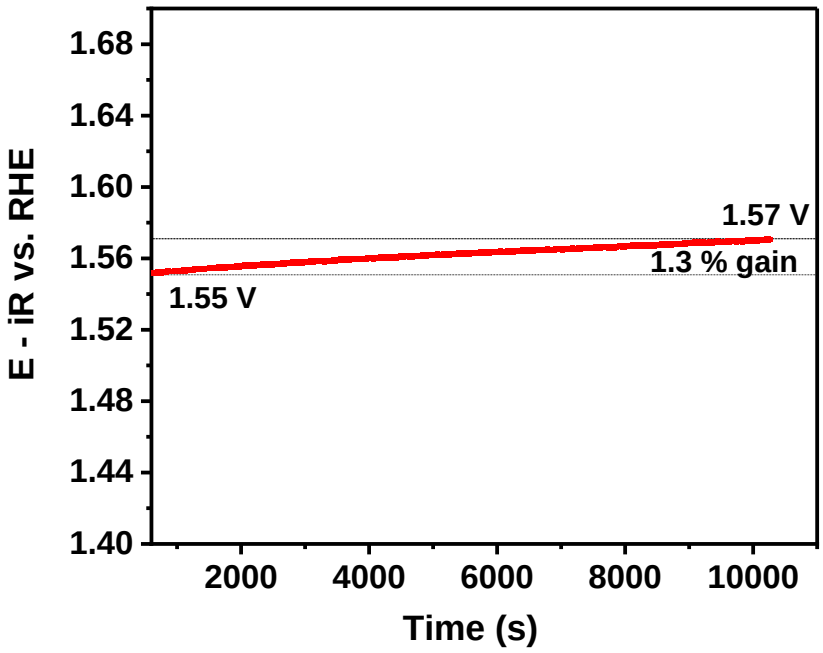

Fig. S49. Long-term potentiometry in 1M KOH for ~ 3 hours at 10 mA/cm^2, showing a minimal gain of 20 mV in overpotential, corresponding to a 1.3 % increase.

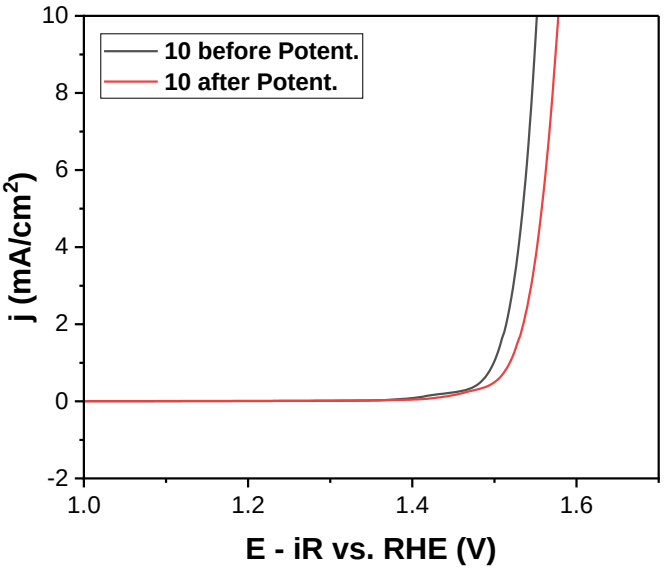

Fig. S50. LSV polarization curves of **10** at 1600 rpm rotation speed and 5 mV s^{-1} scan rate in 1M KOH obtained before (black line) and after (red line) long-term potentiometry.

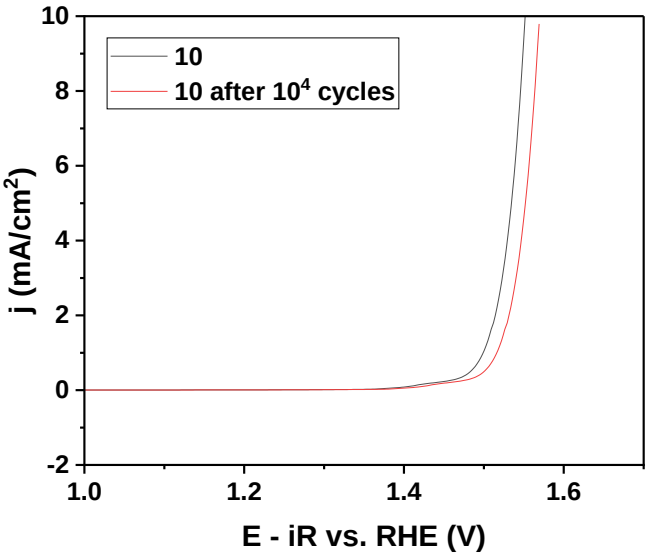

Fig. S51. LSV polarization curves of **10** at 1600 rpm rotation speed and 5 mV s^{-1} scan rate in 1M KOH obtained before (black line) and after (red line) 10^4 cycles.

Material	**Conditions**	**η_{10} (mV)**	**Tafel (mV/ dec)**	**TOF (s^{-1})**	**Reference**
10	0.1 M KOH	350	62	**0.46**	This work
10	1M KOH	320(η_{10}) 500(η_{200})	51	**0.90**	This work
Ni/NiO NPs	1M KOH	337 mV	44	0.20	10.1002/pssb.202200590
NiGe/NF	1M KOH	228	56	-	10.1002/ange.202014331
$Ni_{0.88}Fe_{0.18}O$-1	1 M KOH	340	49	-	10.1021/acsomega.3c00322
Ni_2Si/NF	1 M KOH	η_{100} is 348	50	-	10.1002/aenm.202200269
Ni1.95Fe MOP@CNT	1 M KOH	256	58	-	10.1002/adsu.202000227
Ni45Fe55	0.1M KOH	300 mV	-	0.14	10.1021/jacs.6b00332
Ni3Fe0.5V0.5	1 M KOH	300 mV	-	0.57	10.1038/s41467-018-05341-y
NiFe	0.1 M KOH	320 mV	71-43	0.01-0.20	10.1002/anie.201915803

Table S7. Comparative metrics of highly competitive Ni-based OER electrocatalysts in alkaline media.

References

S1. *J. Am. Chem. Soc.* **2013**, 135 (45), 16977–16987

S2. *Org. Biomol. Chem.* **2013**, 11, 938-954

S3. *Adv. Synth. Catal.* **2014**, 356, 2081-2087

S4. *Eur. J. Inorg. Chem.* **2015**, 8, 1345–1350.

S5. J. Am. Chem. Soc. 2001, 123 (43), 10699-10704.

S6. J. Raman Spectrosc. 2007, 38, 728–736

S7. Carbon 2008, 46, 833–840

S8. Nat. Commun. **2015**, 6, 6616.